Journal of Colloid and Interface Science 642 (2023) 84–99

Contents lists available at ScienceDirect

Journal of Colloid and Interface Science

journal homepage: www.elsevier.com/locate/jcis

Uncovering the mechanisms of cyclic peptide self-assembly in membranes with the chirality-aware MA(R/S)TINI forcefield

Alfonso Cabezón [a], Martin Calvelo [a,b], Juan R. Granja [a], Ángel Piñeiro [c,*], Rebeca Garcia-Fandino [a,*]

[a] Department of Organic Chemistry, Centro Singular de Investigación en Química Biolóxica e Materiais Moleculares (CiQUS), Santiago de Compostela University, CIQUS, Spain
[b] Departament de Química Inorgánica i Orgànica and Institut de Química Teòrica i Computacional (IQTCUB), Universitat de Barcelona, Barcelona 08028, Spain
[c] Soft Matter & Molecular Biophysics Group, Department of Applied Physics, Faculty of Physics, University of Santiago de Compostela, Spain

GRAPHICAL ABSTRACT

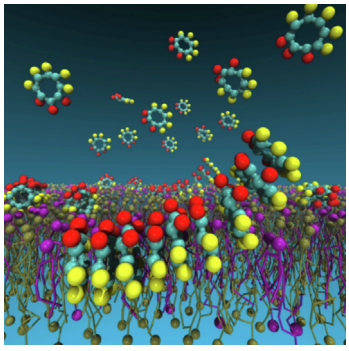

ARTICLE INFO

Article history:
Received 2 February 2023
Revised 19 February 2023
Accepted 16 March 2023
Available online 22 March 2023

Keywords:
Cyclic peptides
Coarse-grained molecular dynamics simulations
Martini forcefield
Lipid bilayers

ABSTRACT

Cyclic peptides (CPs) formed by alternation of *D*- and *L*-amino acids (*D,L*-CPs) can self-assemble into nanotubes (SCPNs) by parallel or/and antiparallel stacking. Different applications have been attributed to these nanotubes, including the disruption of lipid bilayers of specific compositions and the selective transport of ions throughout membranes. Molecular dynamics (MD) simulations have significantly contributed to understand the interaction between CPs, including the structural, dynamic and transport properties of their supramolecular aggregates. The high computational cost of atomic resolution forcefields makes them impractical for simulating the self-assembly of macromolecules, so coarse-grained (CG) models might represent a more feasible solution for this purpose. However, general CG models used for the simulation of biomolecules such as the MARTINI forcefield do not explicitly consider the non-covalent interactions leading to the formation of secondary structure patterns in proteins. This becomes particularly important in the case of CPs due to the *D*- and *L*-chirality alternation in their sequence, leading to opposite orientations of the backbone polar groups on both sides of the cyclic ring plane. In order to overcome this limitation, we have extended the MARTINI forcefield to introduce chirality in each residue of the CPs. The new parametrization, which we have called MA(R/S)TINI, reproduces the expected self-assembly patterns for several CP sequences in the presence of different membrane models, explicitly considering the chirality of the CPs and with no significant extra computational cost. Our simulations provide new mechanistic information of how these systems self-assemble in presence of different lipid scenarios, showing that the CP-CP and CP-membrane interactions are sensitive to the peptide sequence chirality. This opens the door to design new bioactive CPs based on CG-MD simulations. A web-based tool for

* Corresponding authors.
E-mail addresses: Angel.Pineiro@usc.es (Á. Piñeiro), rebeca.garcia.fandino@usc.es (R. Garcia-Fandino).

https://doi.org/10.1016/j.jcis.2023.03.101
0021-9797/

the automatic parameterization of new CP sequences using MA(R/S)TINI, among other functionalities, is under construction (see http://cyclopep.com).

1. Introduction

Molecular self-assembly is the spontaneous organization process of randomly distributed and oriented molecules into well-defined and stable structural arrangements without guidance from an artificial external source [1]. This is mainly controlled by the cooperative result of many weak non-covalent interactions of different type: ranging from electrostatic, direct or water-mediated hydrogen bonds (H-bonds), halogen bonds and van der Waals interactions among others. Nature, through billions of years of evolution, is an excellent reference to find inspiration and ideas for molecular assembly [2]. Unsurprisingly, many scientists have found motivation in the captivating and sophisticated biological recognition mechanisms and they are making an effort to mimic them with diverse organic and inorganic building blocks in the laboratory, with the aim of creating new materials, molecular carriers for active principles or specific molecular traps for toxic compounds, amongst other applications.

Peptides represent one of the most evident organic building blocks for the design of nanomaterials with controllable structural features, due to their simple topology, relative chemical and physical stability, diversity in sequences and shapes, biocompatibility, biodegradability and feasibility to synthesize in large amounts [3,4]. In particular, cyclic peptides (CPs) are a fascinating class of molecules that can be designed, because of their conformationally restricted freedom, to fold or self-assemble into diverse mono- and multidimensional suprastructures with potential applications in biomedicine, nanoelectronics, or catalysis [5–7]. As bioinspired supramolecular building blocks, CPs can stack into self-assembled cyclic peptide nanotubes (SCPNs), which have attracted special attention due to the facility to modify their structure and, thus, their functional properties [5,7]. This makes them well suited to be used in numerous applications, such as electronic devices, artificial photosystems, photoresponsive materials, biosensors, antimicrobials and antiviral agents, selective transmembrane transport channels, catalysis, and drug delivery. The first SCPNs were proposed in 1974 [8], but they could not be synthesized until 1993 [9]. These materials comprised the use of *D*,*L*-α-cyclic peptides (*D*,*L*-α-CPs) formed by an even number of alternating *D*- and *L*-α-amino acids. This leads to a flat ring-shaped conformation in which amide groups (NH and CO) lay perpendicular to the plane of the CPs, allowing the formation of supramolecular nanotubes upon hydrogen bonding with neighbor CPs in a β-sheet fashion (parallel or antiparallel, Fig. 1). Such a special arrangement leaves an empty inner duct of the assembly, with all the side chains exposed on the external surface of the cylindrical structure. One of the main advantages of these nanostructures is the simplicity with which their internal and external properties can be modified based only on the selection of the appropriate CP sequence: the inner diameter of the SCPNs is determined by the number of residues, whereas their outer surface properties depend on the amino acid side chains. The properties and orientation of the SCPN can be tuned by tailoring the peptide sequence [10]. In this sense, SCPNs with appropriate hydrophobic sequences have emerged as attractive transmembrane channel mimics that are able to replicate specific functions of natural transport systems, in terms of affinity, efficiency, stability, and selectivity [11,12]. Alternatively, amphipathic *D*,*L*-α-CPs form SCPNs that lie parallel to lipid membranes causing their disruption, thus making these materials particularly suitable for the development of new antimicrobial agents (Fig. 1A) [13–15].

Molecular self-assembly and, in particular, the assembly of CPs into SCPNs, typically involves a complex interplay of physical interactions that is extremely challenging to investigate with traditional experimental techniques. Different simulation methods can be employed nowadays to model CPs and SCPNs thanks to the currently available computational facilities [16,17]. In particular, Molecular Dynamics (MD) simulations allow to reproduce the self-assembly process of this kind of molecular systems, so it can facilitate unprecedented access to a range of physical properties at the intra-, inter-, and supramolecular scales. While atomic resolution models (AT) can provide important insights into SCPNs [18–25], they are too computationally expensive to follow dynamic behavior of the self-assembly process of CPs. To tackle these limitations, coarse-grained (CG) models, in which multiple atoms are grouped to form joint interaction sites, can be used. Thus, some intramolecular degrees of freedom are ignored to increase the sampling in the system dimensions leading to the spontaneous formation of supramolecular structures. Another advantage of using CG resolution is that the time step employed to solve the motion equations in MD simulations can be significantly increased without losing stability in the calculations. This is because the fastest intramolecular movements are no longer considered at this resolution level, and the shortest periods of the remaining degrees of freedom are typically longer than 100 fs. The immediate consequence of using longer time steps is that significantly longer trajectories, compared to those obtained using AT resolution, can be generated with the same computational resources. Multiscale approaches to take the best from both resolution levels -CG for self-assembly and AT to identify atomic level interactions stabilizing the supramolecular patterns- have been proposed [26].

MARTINI is the most popular CG forcefield for the simulation of biomolecular systems [27–29]. It has been used to investigate the spontaneous self-assembly of peptides, proteins, carbohydrates, surfactants, and polymers into different supramolecular structures. Despite its unquestionable advantages, i.e., reduced computational costs and accurate description of molecular movements, none of the available versions of this forcefield [30–33] considers the non-covalent interactions leading to the formation of secondary structures in peptides and proteins. Secondary structure arrangements are imposed by harmonic potentials between backbone beads. Thus, MD simulations based on MARTINI are not suitable for the study of transitions among different secondary structures, like for example in protein folding. A direct consequence of this limitation is the loss of chirality in the amino acids, and also the lack of information about directional non-covalent forces such as hydrogen, halogen or chalcogen bonds [34], which becomes particularly important in the case of CPs due to the *D*- and *L*-chirality sequential fluctuation: the donor and acceptor groups of each residue (NH and CO) are alternatively oriented in opposite directions with all amide groups of the residues of identical chirality pointing to the same side of the CP plane Due to this directional orientation, D residues of one CP unit interact with L residues of a contiguous, parallel CP, while residues of the same chirality interact in contiguous, antiparallel CPs. (Fig. 1A). Consequently, the self-assembly of *D*,*L*-α-CPs using MARTINI produces a misleading representation of reality because it does not consider these specific interactions, thus making it impossible to distinguish between the parallel

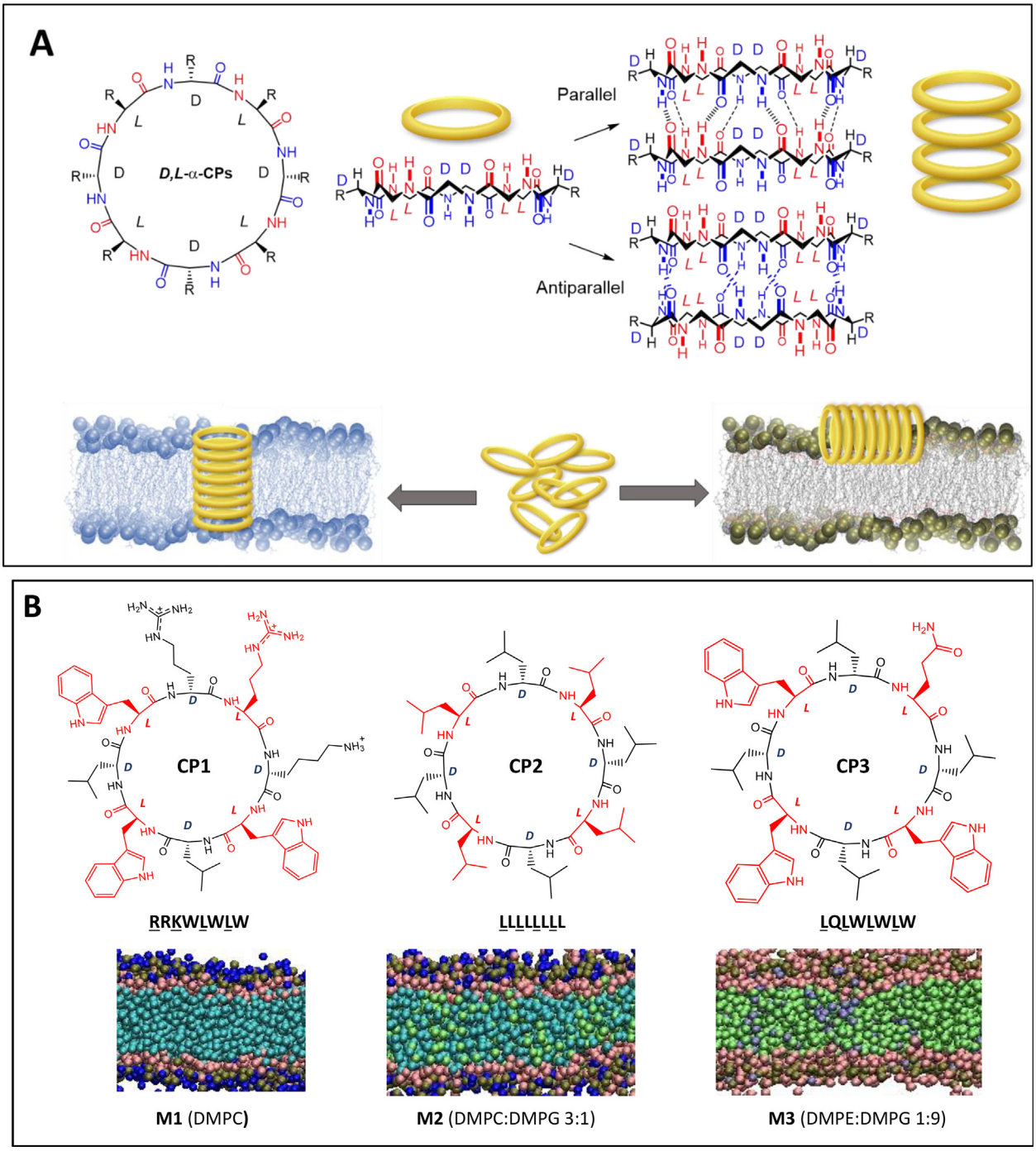

Fig. 1. A. *Top-left*: general structure of a CP, with an even number of alternating *D*- (in blue) and *L*- (in red) α-amino acids. *Top-right*: structure of parallel and antiparallel dimers formed by two CPs, as models of the basic interactions between stacked CPs together with a schematic representation of a SCPN (stacked yellow rings). *Bottom*: schematic representation of a transmembrane channel formed by the self-assembly of hydrophobic CPs (left) and of a SCPN parallel to the membrane formed by amphipathic CPs (right). **B**. *Top*: Structure of the three simulated CPs, **CP1**, **CP2** and **CP3**. The underlined residues in the abovementioned sequences represent the non-natural D-residues. *Bottom*: CG representations of the membrane models **M1** (mammalian), **M2** and **M3** (bacteria), used in this work. (For interpretation of the references to colour in this figure legend, the reader is referred to the web version of this article.)

and antiparallel β-sheets that can be formed along the SCPN (Fig. 2) [7]. Furthermore, the number of possible interactions between backbone beads of different CP units is overestimated, allowing stackings that should be forbidden due to the previously mentioned alternated chirality and alignment (Fig. 2). This overestimation of these interactions is extended not only to all the β-sheet based protein/peptide structures, but also to all the systems where the directionality of the H-bonds is critical, even if the residues have the same chirality. All the CG-MD simulations that have been carried out so far employing MARTINI are subjected to these limitations [13–15,35–37].

In order to solve this problem, an extension of the MARTINI forcefield that introduces chirality in the residues is proposed here. While *ad hoc* CG models might lead, in principle, higher accuracy in

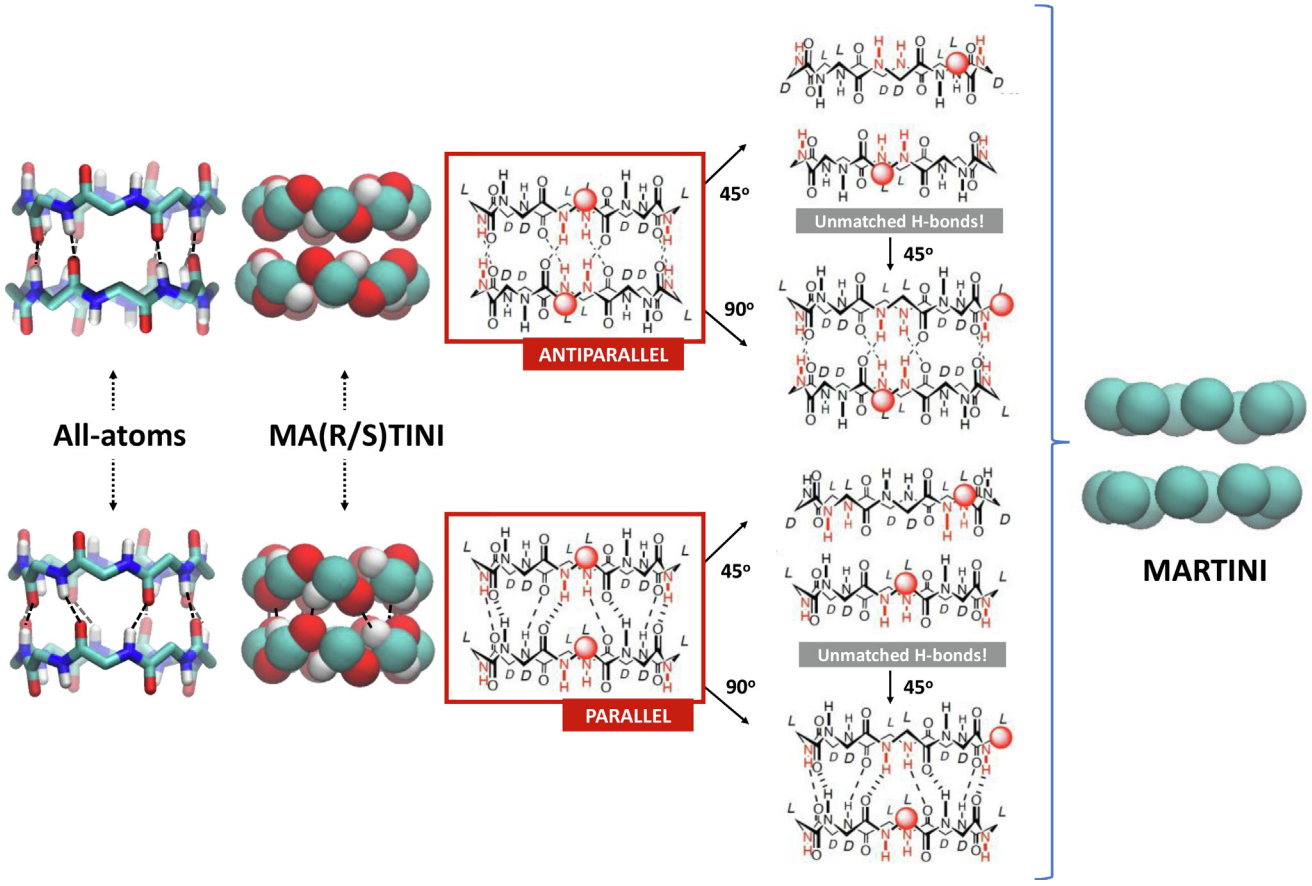

Fig. 2. Atomistic representation of a generalized CP backbone with the optimal antiparallel and parallel conformations of CP dimers, along with a representation of the backbone in the MA(R/S)TINI extension of the force field and the standard MARTINI. Note that standard MARTINI does not account for the limitation of certain orientations, making it impossible to distinguish between parallel and antiparallel β-sheets that can be formed along the SCPN. The "Unmatched H-bonds!" labels indicate that with those relative rotations of both CP units (45°) the formation of H-bonds is not feasible.

the representation and treatment of a specific system, we preferred to extend a well stablished model for which many functional groups have already been parameterized. The new parametrization, which we have called MA(R/S)TINI (Fig. 2), reproduces the expected self-assembly patterns for several CP sequences, explicitly considering the chirality of the CPs with no significant extra computational cost. This strategy facilitates monomer customization as well as the simulation of CPs with relatively complex molecular mixtures: lipid bilayers of different composition, proteins, linear peptides, surfactants, etc. In this way, the self-assembling of monomeric peptides with different sequences can be studied in a variety of environments, allowing to consider structure-activity relationships.

The self-assembly process of three different CP sequences in the presence of membrane models for healthy mammal and for bacteria has been simulated using the classical and the new parameterizations of the MARTINI forcefield (Fig. 1B). The three CPs are expected to exhibit different behaviors in the presence of the employed membrane models due to the large differences in the total charge, as well as in the hydrophobic and electrostatic dipolar moments. The MA(R/S)TINI parameterization reproduces the general trends expected for the proposed sequences while it explicitly considers the chirality of the CPs that is missed in the original MARTINI model. Furthermore, the simulations with the new parameterization provide new mechanistic information of how these systems self-assemble in presence of different membranes, at a level of resolution that had not been previously attained.

2. Materials and methods

2.1. Peptide sequences and membrane models

Three cyclic sequences of 8 amino acids each, with different expected behaviors in the presence of a lipid environment, were used (Fig. 1B): **CP1** (RRKWLWLW), with amphipathic character and with demonstrated activity against bacteria [38]; **CP2** (LLLLLLLL), consisting on a fully hydrophobic sequence so, a priori, it should lead to the formation of transmembrane SCPNs; and **CP3** (LQLWLWLW), mostly hydrophobic and known to form transmembrane nanotubes [11]. The underlined residues in the abovementioned sequences represent the non-natural D-residues.

These CPs have been simulated in the presence of three different lipid membrane models, depicting a mammalian and two bacteria cell membranes (Fig. 1B). The mammalian model (**M1**) consisted of a pure 1,2-dimyristoil-*sn*-*glycero*-3-phosphatidylcholine (DMPC) bilayer, as this lipid represents >50% of the phospholipids in most eukaryotic membranes [39]. The bacterial membrane models (**M2** and **M3**) were formed by a mixture of 1,2-dimyristoyl-*sn*-*glycero*-3-phospho-(1′-*rac*-glycerol) (DMPG) and DMPC in 3:1 ratio for **M2** and 1,2-dimyristoyl-*sn*-*glycero*-3-phosphoethanolamine (DMPE) and DMPG in 1:9 ratio for **M3**, since these lipids are the main constituents of Gram-Negative and Gram-Positive bacteria membranes [40,41]. These models are expected to provide useful information about the role of lipid composition, and

in particular of the net charge of the membrane, in the self-assembly of the CPs.

2.2. Structure and parameterization of the CPs

The coordinates of the particles describing the CP models and the corresponding force field parameters (topologies) were generated as follows:

2.2.1. Standard MARTINI

Atomistic coordinates of linear peptides with the required sequences are automatically obtained using the Python *PeptideBuilder* library [42]. The resulting structures are then mapped into a MARTINI v2.2 CG model [43] with the *martinize.py* tool [31]. Next, following the Tarek's strategy [37], the topology provided by this tool is modified by introducing the bonds, angles and dihedrals that reproduce a reliable structure for the CPs: The bonds between backbone beads (BB) are described by a harmonic potential with the equilibrium distance at 3.8 Å and a force constant of 6275 $kJ{\cdot}mol^{-1}{\cdot}nm^{-2}$. The angle between consecutive BB beads is described using again a harmonic potential with an equilibrium angle θ_0 of 135° and a force constant of 627 $kJ{\cdot}mol^{-1}{\cdot}rad^{-2}$. Improper dihedrals centered on each BB and using the corresponding lateral chain together with the two bound BB beads are imposed to restrain the relative orientation of each residue. The angle and force constants employed in this case are ξ_0 = 180° and K_ξ = 418 $kJ{\cdot}mol^{-1}{\cdot}rad^{-2}$. A second group of improper dihedrals between 4 consecutive BB beads with an equilibrium angle of 0° and the same force constant employed above (418 $kJ{\cdot}mol^{-1}{\cdot}rad^{-2}$) is added to restrain the planarity of the CPs. All these parameters were directly taken from the Tarek's previous work [37], with the exception of the force constant for the bonds between BB beads, In order to increase the rigidity of these interactions and enhance the stability of the simulations, such force constant was augmented by a factor of 100. The resulting structures and parameters were taken as a reference to include the chirality in the extended version of the forcefield (see below).

2.2.2. MA(R/S)TINI parameterization

To introduce chirality in the *D*- and *L*- residues composing the CPs, the original P5 bead representing the backbone in the classical MARTINI CG model was replaced by a new particle (CPBB) combined with two virtual sites (CPCO and CPNH). The virtual sites (VS) were introduced to depict the C═O acceptor (CPCO) and N—H donor groups (CPNH) of the amino acids (Fig. S1). The parameters associated to the new beads (σ and ε values for the Lennard-Jones potential, equilibrium distances, angles, and force constants) were optimized through an extensive trial and error iterative process in which several tens of combinations were essayed. The criterion utilized for the determination of the optimal LJ parameters was guided by a purely empirical approach, which involved screening a large number of potential combinations until the most favorable ones were identified. The final values lead to both parallel and antiparallel SCPNs with the experimentally reported distances between CPs and the expected interactions between the VS (Fig. 2) [9,11]. This extension of the MARTINI force field was designed to maintain the versatility of its original version, so the modifications only affect the interaction between CPs. Thus, the new CPBB bead has exactly the same parameters as the original P5 MARTINI particle, including the cross-interactions with all the beads of the force field. However, the σ Lennard-Jones (LJ) parameter for the CPBB-CPBB self-interaction was decreased from 0.47 to 0.4 Å. This reduction was key to get a CP-CP distance closer to the experimentally reported by electron diffraction and Fourier-transformed infrared spectroscopy values [9,11], compared to the original version of the force field (see below). On the other hand, VS were used to model the C═O and N—H groups, thus introducing chirality in the CG model of the CP, directly keeps them at fixed positions with respect to the backbone. *3out* type VS, as defined in GROMACS [44], were employed for both CPCO and CPNH. This means that the position of each VS is given by a set of coordinates in a local reference system given by three beads. The position in the plane and out of the plane defined by such beads can be easily set in the topology file. Trying to mimic the optimized atomic structure of the CPs, both VS particles, CPCO and CPNH, were initially placed at 1/3 of the distance between consecutive BB beads (*d*), along the axis joining them (Fig. S1). This distance was set to 0.35 *d* upon optimization. A similar process was followed to get the distance to the central bead (CPBB) in the vertical axis (*h*), obtaining a value of 1.053 Å (which is the length of the N—H bond in atomic resolution models) for both VS. This distance, combined with the reduced σ value of the CPBB beads, is key to define the distance between CPs in SCPNs. In contrast to CPBB, the new CPCO and CPNH particles are allowed to interact only between them. The self-interaction parameters are σ = 0.35 nm and ε = 3 $kJ{\cdot}mol^{-1}$, leading to a relatively weak interaction, while the cross-interaction is much stronger: σ = 0.26 nm and an ε = 5.6 $kJ{\cdot}mol^{-1}$.

2.3. Construction of the lipid bilayers

CG lipids distributed in 250 units per leaflet were introduced in a 12.5x12.5x15 nm^3 rectangular simulation box and solvated using the MARTINI Builder module of the CHARMM graphical-user interface [45] (Fig. 1B).

2.4. Free MD simulations

Once the CP structures were optimized for both parametrizations (standard MARTINI v2.2 and MA(R/S)TINI), different number of CPs (20, 40, 80 and 160) were inserted into the water phase of the simulation boxes corresponding to each of the three membrane models. As a result, 36 systems (3 membrane models × 3 CP sequences × 4 CP concentrations) were prepared. The counterions required to neutralize the electrostatic charge of the whole system were added in each case. A steepest descent energy minimization was performed to remove eventual atomic overlaps and clashes, followed by 50 ps (for simulations in MARTINI) and 50, 200, 2500, and 1500 ps (for MA(R/S)TINI) of stepwise constant pressure equilibrations using the Berendsen barostat [46]. The production trajectories were carried out at 1 bar and 303 K using the semi-isotropic Parrinello–Rahman barostat [47], and a V-rescale thermostat [48]. The LINCS algorithm [49] was used to eliminate bond vibrations or its drifting in the system. The Particle Mesh Ewald [50] method with periodic boundary conditions was used to treat the long-range electrostatics with a 1.1 nm cut-off in direct-space. The dielectric constant was set to 15, as recommended for the non-polarizable version of MARTINI [51]. Van der Waals interactions were computed using a spherical cut-off of 1.1 nm. Production trajectories of 20 μs with a time step of 25 fs (for the MARTINI model) and 20 fs (for the MA(R/S)TINI model) for the integration of the motion equations were performed. Energies and positions of atoms were stored every 1000 steps (25 ps). All MD simulations were performed with the GROMACS 2021.4 [52] software package.

2.5. Metadynamics simulations

Parallel and antiparallel CP dimers were built for both MARTINI parameterizations (standard v2.2 and MA(R/S)TINI versions of the forcefield). Each system was subjected to a 500 ns free MD simulation following the protocol described above, in all cases the dimers remain stable. Then, well-tempered two-dimensional metadynam-

ics simulations with PLUMED 2.8.0 [53] and GROMACS 2021.4 [52] were performed at 298 K, using the distance between the centre of mass of both dimers and the relative angle between the vectors joining the centre of each CP with its own first BB bead as collective variables. This angle measures the relative rotation between CPs while they share the same symmetry axis (perpendicular to the plane of the peptide ring). Gaussians with 0.1 kJ mol^{-1} height and 0.01 nm width were deposited every 500 ps using a biasing factor of 15. Several harmonic restrains were applied to the relative movement of both CPs: the angle between the normal to the CP rings was set to 0° for parallel dimers and to 180° for antiparallel structures; and the centres of mass were restrained to move throughout the axis perpendicular to both CPs, with no lateral displacement. The force constants used for both restraints was 1000 kJ mol^{-1} rad^{-2} for the angle and kJ mol^{-1} nm^{-2} for the distance to the axis. An artificial wall was also set to prevent a separation longer than 2.5 nm between the centre of both CPs. A minimum of 10-μs-long trajectories with 6 walkers were obtained following this protocol.

2.6. Analysis of the trajectories

VMD [54] was employed to generate snapshots and animations from the MD trajectories. The analysis of the simulations was carried out using GROMACS and PLUMED tools as well as specific code written in Python mainly based on the MDAnalysis [55], NumPy [56] and Matplotlib libraries [57].

For the free simulations, the number of CPs forming nanotubes of different size was computed as a function of time. For the kinetic analysis, two CPs are considered to form a dimer when the distance between their centres of mass is lower than 6 Å. This analysis allows to observe the spontaneous self-assembly of independent CP molecules, as well as their interaction with the different membrane models, since they are initially at random positions and orientations within the simulation box. Average values of the following properties along the last microsecond of the trajectories were determined: the number of CPs forming parallel and antiparallel dimer β-sheets, the distance between the centers of mass of the same CPs, and their rotational angles. For this analysis a more restrictive cutoff of 5.5 Å was employed to consider that two contiguous CPs form a dimer. The parallel and antiparallel orientations of contiguous molecules are identified from the angle between the normal vectors to the CP rings (Fig. S2). These normal vectors are determined considering the closest plane to the 8 CPBB beads of each CP, and they are clockwise oriented in the direction defined by the residue sequence. Then, the angle for parallel and antiparallel relative orientations are expected to be 0° and 180°, respectively.

Potential of mean force (PMF) profiles were obtained from the 2D metadynamics simulations using the *sum_hills* tool of PLUMED [53].

3. Results and discussion

3.1. Validation of the MA(R/S)TINI parameters: Potential of mean force profiles for parallel and antiparallel CP dimers

In order to evaluate the reliability of the MA(R/S)TINI parameters, metadynamics simulations (see Methods) were carried out for parallel and antiparallel dimers with the three selected CPs (**CP1-CP3**). The objective of the metadynamics simulations is to quantify the energy of interaction between CP dimers as a function of the distance between the center of mass of CP units, of the rotational angles and also of the relative orientation between them (parallel or antiparallel). The MA(R/S)TINI parameters led to significantly more reliable results than the original MARTINI parameterization in all the studied cases. The resulting energy profiles (Fig. 3) clearly confirm: (*i*) the minimum energy for all peptides and for both the parallel and the antiparallel orientations corresponds to a shorter distance between CP units using MA(R/S)TINI than using MARTINI; (*ii*) only 4 rotational angles centered at 0°, 90°, 180° and 270° are allowed for the new chirality aware parameterization while for the original MARTINI parameterization 8 angles are observed; (*iii*) the rotamers observed for the original force field are shifted by 22.5° with respect to the expected angles; and (*iv*) in contrast to the new parameterization, MARTINI is not sensitive to the relative orientation (parallel or antiparallel) of the CP units. In addition to this information, several interesting features can be seen in the PMF profiles. First, both parameterizations exhibit periodic energy barriers of decreasing amplitude as the distance between both CPs increases. Such energy barriers arise from the solvation layers with the explicit water beads considered in the force field, which are identical for both parameterizations (Fig. S3). This behaviour is reflected in the 2D PMF profiles as vertical bands of different intensity. In the 1D projection of the PMF on the distance between CPs, the solvation layers are seen as damped waves with one or more small shoulders along the first period (Fig. 3). Those shoulders are provoked by the impact of the rotamers in the first solvation layer. Such effect is clearer for the original MARTINI probably because for that parameterization there are twice more rotamers than for MA(R/S)TINI. This behaviour is clearly observed for the three CPs and for both relative orientations (Figs. S4-S8). Notably, MA(R/S)TINI distinguishes better the sequence than MARTINI. More specifically, the depth of the minima for **CP1** and **CP3** are more similar to each other than those for **CP2**. This happens for both parameterizations and relative orientations, but the differences are clearer for the new parameterization (see Table 1). The energy values in Table 1 also show that the parallel orientation is slightly preferred over the antiparallel one when using the MA(R/S)TINI model while the PMF profile is much more similar for both relative orientations of the CP units for old parameterization of the force field. The anisotropy of the rotations is only marginal in the metadynamics simulations in pure water, in contrast to what is observed in the unbiased free MD simulations (see section 3.2.3). This indicates that the external presence of the membrane model favours specific rotations of the CPs, more than the interaction between contiguous CPs.

3.2. Self-assembly of CPs into SCPNs

Once it is confirmed that MA(R/S)TINI reproduces the correct relative rotations between CP dimers, unbiased MD simulations using 20, 40, 80 and 160 CP units in the presence of three different membrane models (**M1-M3**), were carried out for all the sequences (**CP1-CP3**). The results of the analysis obtained from all these simulations are presented in what follows.

The presence of lipid membranes in the simulation boxes represents a double-edged sword for the self-assembly of CPs into SCPNs. On one hand, the lipid membranes may compete with CP aggregates for the capture of peptide monomers, hindering the formation of SCPNs in aqueous media. On the other hand, the lipid bilayers can also help the self-assembly of CPs by attaching individual molecules to their surface, increasing their local concentrations and potentially aiding the formation of SCPNs embedded in membranes. The interaction mechanism of the CPs or the corresponding nanotubes with the lipids will be determined by the nature of the amino acids in each sequence. As mentioned in the Methods section, **CP1** is expected to form horizontally oriented SCPNs in the lipid membrane due to its amphipathic character, while **CP2** and **CP3**, are expected to form transmembrane nanotubes because of their hydrophobic sequences.

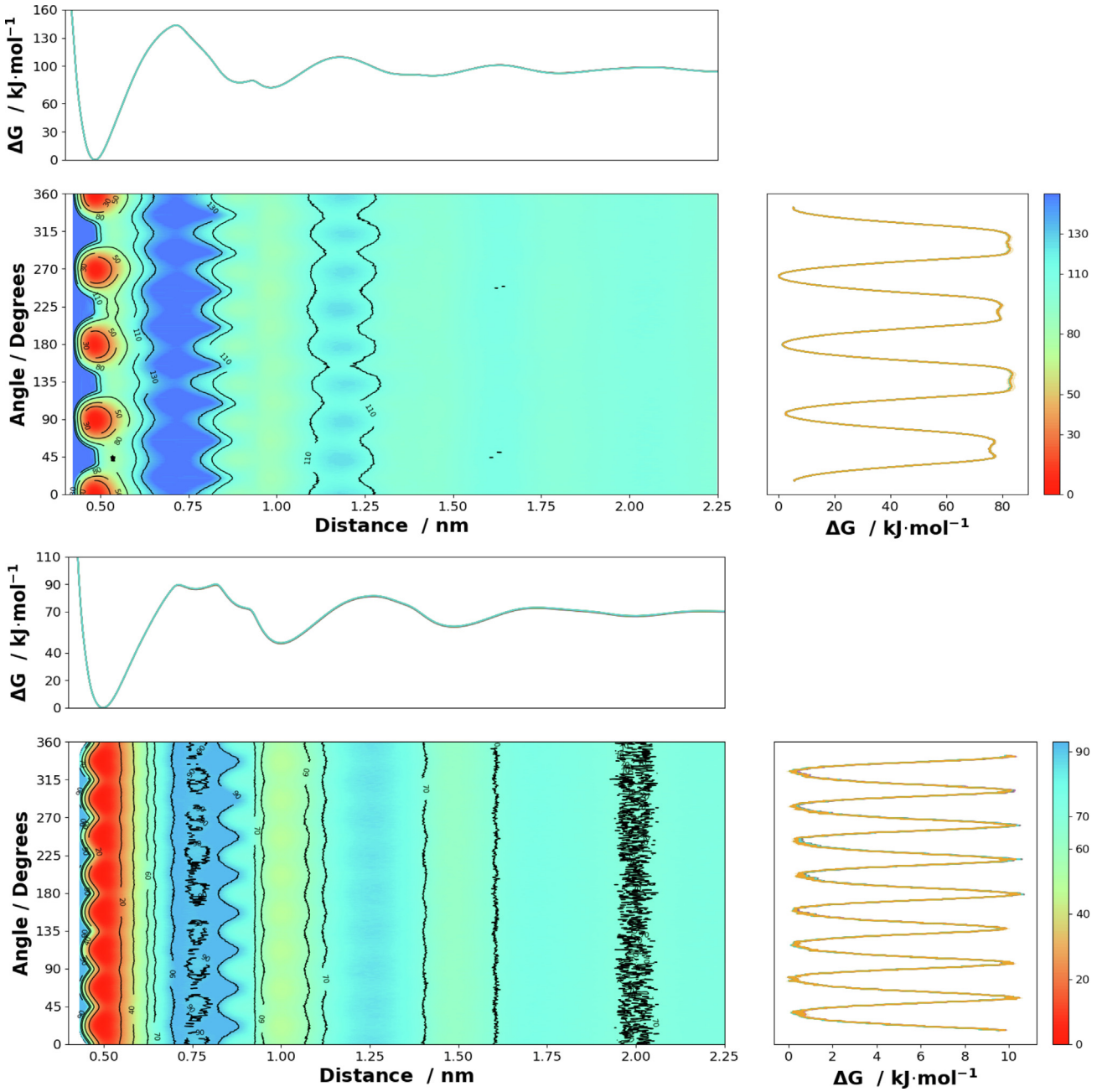

Fig. 3. Two-dimensional potential of mean force (PMF) profiles obtained for the interaction between **CP2** dimers with antiparallel relative orientation from metadynamics simulations (see Methods section) using the MA(R/S)TINI (*top*) and the MARTINI (*bottom*) models. The 1D projections of the PMF on each collective variable (distance between CP units and rotational angle) calculated over periods of 0.8 μs is shown on top and on the right of the PMF plots. The results obtained for all the sequences and orientations are shown in Figs. S4-S8.

Table 1
Energies (in kJ/mol) and their corresponding standard deviation (between parenthesis), corresponding to the flat region in the one-dimensional projection of the PMF profile on the first collective variable (the distance between monomers) for the 3 CPs with both relative orientations and parameterizations of the force field. These energies represent a measurement to the depth of the lowest minima with positive sign.

	MA(R/S)TINI				MARTINI			
	Parallel		Antiparallel		Parallel		Antiparallel	
CP1	159	(17)	115.6	(7.0)	76.7	(5.3)	75.7	(5.4)
CP2	115	(16)	101.9	(7.0)	67.1	(4.0)	66.7	(3.4)
CP3	154	(21)	114.6	(7.6)	78.5	(5.0)	78.6	(5.9)

The membrane models, CP structures and concentrations chosen for the free simulations are intended to provide insight into the ability of both MARTINI and MA(R/S)TINI force fields to accurately represent not only the ability to form nanotubes but also to anticipate trends for each system. The kinetic variation in cluster sizes over the whole trajectories, as well as the distributions

between parallel and antiparallel CP arrangements, CP-CP distances and rotational angles for contiguous CPs in the last microsecond of each trajectory, will be used as quantitative descriptors of the self-assembly process and the resulting final supramolecular structures.

3.2.1. Kinetics of the simulations and SCPN length distributions

In all cases, the distribution of CPs in aggregates of different sizes was stable before the end of the trajectories (20 μs long). This analysis revealed significant differences based on the peptide sequence and on the lipidic environment sensed by the CPs (Fig. 4 and S9-S15). The results of the simulations in the presence of different membrane compositions are discussed separately in the next section:

*3.2.1.1. Simulations in the presence of DMPC bilayers (**M1**).* The results of the simulations containing 40 CP units and using the MA(R/S)TINI model are shown in Fig. 4. It is observed that, even after 20 μs, a significant number of **CP1** and **CP3** monomers remain as independent entities in the corresponding simulation boxes, while for the simulation with **CP2** almost all the peptides become part of trimers or larger aggregates within the first 7 μs. The distribution of **CP1** molecules between SCPN of 1–5 molecules (monomers to pentamers) is quite homogeneous, ranging from 5 to 10 units per type of assembly over the last 10 μs of the trajectory. The last few μs contain 6 monomers, 5 dimers, 2 trimers, 2 tetramers and 2 pentamers. **CP2** clearly forms larger and very stable aggregates, the last 14 μs with 2 dimers, 5 trimers, 1 tetramer, 2 pentamers and even 1 heptamer, with no monomers at all. The behaviour of **CP3** is more similar to **CP1** than to **CP2**, the last few μs containing 9 monomers, 8 dimers, 2 trimers, 1 tetramer and 1 pentamer. Similar general trends, although with some singularities, are observed at other peptide concentrations. **CP2** still exhibits a higher ability to aggregate, compared to **CP1** and **CP3**, in all the simulations. For the simulations with 20 CP units, **CP1** still shows several free monomers together with some dimers, trimers, and a longer SCPN; **CP2** forms 3 hexamers, together with some dimers and trimers; and **CP3** forms mostly trimers, together with a pentamer and several dimers (Fig. S9). The simulations with 80 peptide units (Fig. S12) are more similar to those with 40 CPs. **CP1** and **CP3** form relatively small aggregates (mostly dimers and trimers) while **CP2** forms predominantly tetramers, pentamers, hexamers and even heptamers. In the simulations containing 160 peptides, a large number of **CP1** and **CP3** remain as monomers at the end of the corresponding trajectories while **CP2** tends to form SCPNs of 4 to 8 units (Fig. S14).

For the simulations with the original MARTINI model using 40 CP units, **CP2** and **CP3** form medium sized SCPNs, while the behaviour of **CP1** is more similar to that observed with the new parameterization (Fig. S11). The main assemblies observed in the trajectories with 20 CPs are again dimers and trimers for **CP1**, **CP2** leads to one trimer, 2 pentamers and even one heptamer, and **CP3** forms an octamer together with trimers and dimers (Fig. S10). When using 80 CP units, dimers and trimers are mostly formed for **CP1** and **CP3**, while the assemblies with **CP2** are larger, with SCPNs of 6, 9 and even 11 molecular units, and with no dimers and trimers at all (Fig. S13). Finally, the simulations with 160 units of **CP1** and **CP3** are again similar to those obtained with their respective studies in the new parametrization, being monomers, dimers and trimers the dominant species. **CP2** changes its tendency a bit as the nanotubes formed are not as large as with the other concentrations, now 4-subunit SCPNs are predominant followed by dimers and trimers (Fig. S15).

*3.2.1.2. Simulations in the presence of DMPC:DMPG 3:1 bilayers (**M2**).* The behaviour of the peptides in this model of bacteria membrane is quantitatively different from that in the simulations with pure DMPC lipid bilayer (**M1**) but the general qualitative features persist. Again, for the simulations using 40 CP units with the MA(R/S)TINI parameterization, a significant number of **CP1** and **CP3** monomers survive as independent molecules while all the **CP2** molecules aggregate forming medium size SCPNs (Fig. 4).

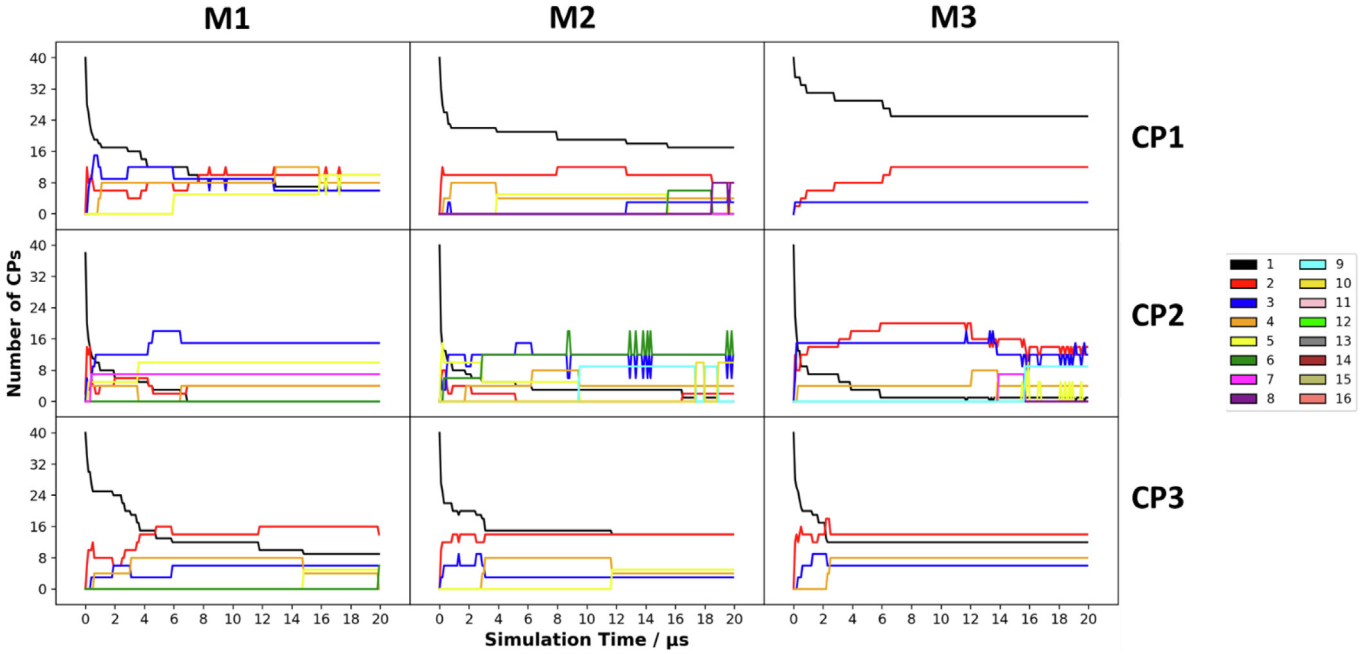

Fig. 4. Number of CPs in clusters of different size (indicated by the colours in the legend) as a function of time, for simulations with 40 units of **CP1**, **CP2** and **CP3**, in presence of the three membrane models, using the new MA(R/S)TINI CG parameterization developed in this work. Note that the initial value (at Time = 0) corresponding to the black line (representing the number of monomers) is always 40 for all the plots, while the rest of the lines start at zero. The exchange of CPs between clusters of different size can be clearly seen in the behaviour of the different curves. The results obtained for the rest of the free MD simulations with different number of CP units are in Figs S9-S15.

The main quantitative difference is apparent for **CP1**, which shows a significantly larger number of monomers in the presence of this membrane than in the presence of **M1**: almost half of the peptides remain stable as independent structures and the rest of molecules form mostly dimers. The differences in the behaviour of **CP2** and **CP3** between the two membrane models are less clear. The trends of the simulations with 20 CP molecules are similar (Fig. S9), or even more marked than those using 40 peptide units. More than half of **CP1** remain as monomers after 20 μs while no isolated **CP2** molecules and just one dimer was found in the corresponding simulation and an intermediate behaviour is observed for **CP3**, with 6–7 stable monomers and a similar number of peptides assembled in dimers, trimers and one tetramer. Again, the dominant species are **CP1** monomers when using 80 peptide units, medium size SCPNs for **CP2** and a significant presence of monomers and mostly dimers for **CP3** (Fig. S12). Monomers, dimers and trimers dominate the simulations of 160 **CP1** and **CP3** while SCPNs with 3 to 5 units are more likely for **CP2** (Fig. S14).

The simulations using the original MARTINI force field seem to favour the aggregation kinetics, compared to the results obtained using MA(R/S)TINI. The final number of **CP1** monomers after 20 μs in the simulation with 40 peptide units is lower than that with the new parameterization, although most of the aggregates are small dimers and trimers (Fig. S11). A similar behaviour is observed for **CP3**, although for this peptide the SCPNs are a bit longer. **CP2** exhibits a faster kinetics, reaching stable tetramers and pentamers just after 3 μs. Reducing the number of components to 20 in the simulation boxes, the three systems conserve the trends: **CP1** forms small aggregates and less monomers than in the simulations with the new parameterization; **CP2** forms longer aggregates of up to 9 subunits and, surprisingly, **CP3** leads to an aggregate of 16 peptides that includes most of the CPs in the simulation box (Fig. S10). Differences between both parameterizations are smaller when the concentration of peptides increases up to 80 peptide molecules (Fig. S13). Slightly less monomers and more **CP1** dimers are formed with MARTINI than with MA(R/S)TINI, 2 to 5 units length SCPNs are quickly formed with **CP2**, and **CP3** is mainly distributed in monomers and dimers, with 3 trimers, 6 tetramers and even one hexamer at the end of the trajectory. For the simulations with 160 peptides (Fig. S15), the final distribution of structures is similar for **CP1** and **CP3**, with most of the peptides as monomers, dimers and trimers, while **CP2** aggregates much faster and forms significantly larger aggregates of up to 9 molecular units.

*3.2.1.3. Simulations in the presence of DMPE:DMPG 1:9 bilayers (**M3**).* The simulations with this lipid bilayer are characterized by a larger presence of **CP1** monomers for both parameterizations of the force field, compared to the simulations with the other two membrane models. This is likely due to the electrostatic attraction between this cationic peptide and the DMPE:DMPG 1:9 bilayer (**M3**), which contains a high density of anionic lipids.

Thus, the **CP1** structures directly join the membrane as monomers, making difficult their aggregation. Typically, half of the **CP1** structures remain as monomers throughout all the simulations, regardless the concentration and even of the force field parameterization, while the rest of the peptide units form mostly dimers and some trimers, also interacting with the membrane (Fig. 4 and S9-S15). **CP2** keeps its ability to aggregate very quickly compared to **CP1** and **CP3**, forming relatively large SCPNs of up to 8–10 peptide units for both parameterizations and for all the concentrations. Again, a key feature of **CP3** is the persistency of monomers even at large concentrations of the peptide for both parameterizations. This behaviour is a constant for both **CP1** and **CP3**, although to a lower extent for **CP3**.

Differences in the kinetic behaviour between both force field parameterizations are not evident for any of the three CP sequences. The general trends are also similar, although quantitative differences can be observed. The behaviour of **CP1** in the simulation with 20 peptide units is practically the same for both parameterizations (Fig. S9-S10) while for the rest of concentrations the ratio of CPs forming dimers to the number of monomers is higher for the original MARTINI parameterization than for MA(R/S)TINI (Fig. 4 and S11-S15). **CP3** also exhibits a persistent higher number of independent peptide units in the simulations with the new parameterization of the force field for all the studied concentrations. **CP2**, in agreement with the simulations in the other two membrane models, does not show free monomers at the end of the trajectories but the final aggregates are consistently larger at all the concentrations for the simulations with the original MARTINI force field.

Overall, the kinetic analysis reveals interesting aspects on the competition between the adsorption of the peptides by the lipid bilayers and their self-assembly process. It is shown that the self-assembly kinetics is significantly faster for **CP2** in practically all cases. This is probably connected to a specific interaction mechanism exhibited by this peptide (see next section). The self-assembly of CPs and the interaction with the lipid bilayers are seriously affected by the electrostatic attraction between different molecular entities (CP monomers, CP aggregates and membrane models). This is very clear for the most cationic peptide (**CP1**), which exhibits a progressively lower tendency to self-aggregate when increasing the negative charge density of the membrane, thus favouring its adsorption. It can be shown that the hydrophobic residues (W and L) of all the CPs in the SCPN are oriented towards the same side of the CP assemblies using both MA(R/S)TINI and MARTINI (Fig. S16). When a lipid membrane is present, these hydrophobic residues interact with the lipid tails of the bilayer, while the ionic residues (R and K) are exposed to the polar solvent. One difference between these two forcefields is that with the new parametrization, the formation of an amphipathic SCPN, i.e., with polar and nonpolar residues aligned with themselves, seems to be less likely in the absence of the membrane. This means that the relative orientation of the residues is more random with MA(R/S)TINI than with MARTINI in aqueous media. Additionally, the length of the final SCPNs is also consistently larger for the neutral **CP2** than for the charged **CP1** and, to a lower extent for the polar **CP3**. Globally, no significant quantitative differences can be observed between MARTINI and MA(R/S)TINI in terms of the number of CP clusters formed during the simulated time (Fig. 5).

3.2.2. Final self-assembly patterns

The kinetic quantitative results are clearly connected to the final self-assembly patterns achieved by each system (Fig. 6). When using the chirality aware MA(R/S)TINI force field in presence of the mammalian membrane model (**M1**), the cationic **CP1** and the non-ionic but polar **CP3** tend to aggregate in the aqueous solution more than to interact with the neutral lipid bilayer, while **CP2** clearly exhibits two different interaction mechanisms: formation of SCPNs throughout the lipid membranes and formation of two-dimensional lattices in water solution. This behaviour persists for all the peptide concentrations. In contrast, **CP1** is strongly attracted for both bacteria membrane models (**M2** and **M3**) favoured by electrostatic interactions. When the concentration increases, **CP1** seriously perturbs the structure of such membrane models, mainly that of **M3**, indicating the specificity of this peptide towards membranes of different composition and, in particular, charge density. These results suggest the interaction mechanism for the toxicity of **CP1** towards bacteria. The simulations using the original MARTINI force field provide similar results to those obtained with the MA(R/S)TINI parameterization (Fig. S17). At low concentrations

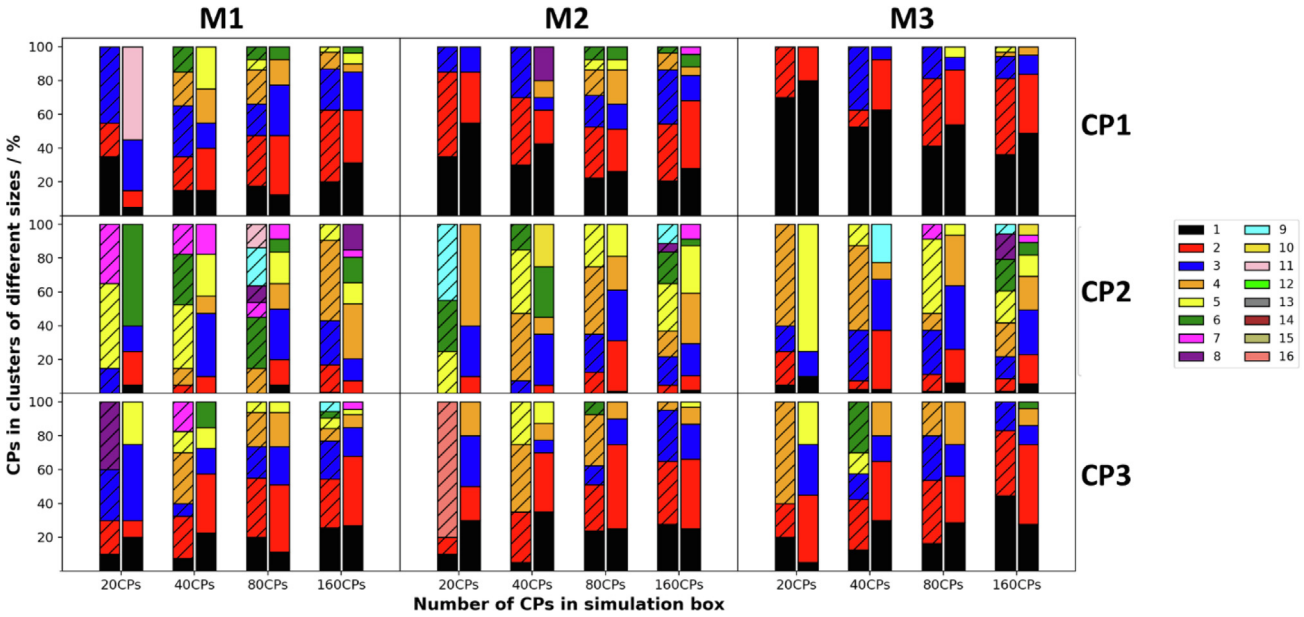

Fig. 5. Number of CPs in clusters of different size (indicated by the colours in the legend) for the last frame of all the CPs and membrane models (indicated in the labels). The results for the simulations with the original MARTINI parameterization are represented as the striped bars while those for the new MA(R/S)TINI parameterization are represented as solid bars.

CP1 interacts with the surface of **M1** while at higher concentrations it aggregates mainly in the aqueous solution. Again, this peptide has a strong affinity to interact with bacteria membrane models, causing significant distortion of **M3** membranes and, to a lesser extent, of **M2**-type membranes at high concentrations.

The electrostatically neutral and hydrophobic nature of **CP2** suggests that this peptide should not be too affected by the lipid composition of the membrane. Considering its sequence, it is expected to self-assemble at the membrane hydrophobic environment into transmembrane SCPNs, independently of the membrane model used in the simulations, although no experimental information is available for this system [58]. Our free simulations confirmed this prediction for **CP2** in presence of the three membrane models, mainly at low concentrations of peptide for **M1**, intermediate concentrations for **M2** and high concentrations for **M3** (Fig. 6). Notably, the formation of two-dimensional lattices with the CPs interacting throughout lateral leucine zippers, is observed in the presence of the three membrane models, mainly at high concentrations of the peptide. This kind of structures have been recently observed by scanning transmission electron microscopy using the so called CPx (which consists of the following residues: WLHEQHEL) [59]. The kinetics of this structural pattern seems to be significantly faster than the less ordered aggregation exhibited by the other two peptides in aqueous solution. It is worth to mention that the 2D lattices observed at high concentrations are large enough to be connected in an infinite plane by periodic boundary conditions (PBCs), but it is also observed at low concentrations with just a few units (see simulation with 40 units of **CP2** in the presence of **M1**, for instance, Fig. 7) discarding that this pattern is an artifact caused just by the PBCs. It seems that the formation of this pattern competes with the formation of transmembrane SCPNs, the kinetics favouring the 2D lattices. Thus, at high concentration of the peptide, the aggregation in the aqueous solution dominates and less nanotubes are observed, which could also be related to the low solubility and tendency to precipitate that has been observed experimentally for these CPs. Again, no significant differences in the general aggregation pattern between both parameterizations of the force field are observed, including the spontaneous formation of the 2D lattices (Fig. 6 and S17).

As in the kinetic analysis, the behaviour of **CP3** is closer to that of **CP1** than to **CP2**. **CP3** does not form transmembrane nanotubes and leads to relatively disordered aggregates in aqueous solution but, in contrast to **CP1**, does not distort any of the membrane models. The membrane composition, the concentration of the peptide and the force field parameterization do not seem to significantly affect the interaction mechanism nor the aggregation pattern (Fig 6 and S17). The reason for the lack of transmembrane nanotubes in MD simulations of **CP3** is unclear. One possible explanation is the presence of an energy barrier that prevents the membrane penetration along the simulated time period. As a non-charged and slightly polar nanotube, it is relatively comfortable in the aqueous phase but it may be difficult to cross the interface formed by the lipid polar heads to enter into the hydrophobic region of the lipid bilayer. In any case, simulating a pre-formed nanotube inside the membrane resulted in the preservation of the transmembrane structure and orientation using the MA(R/S)TINI force field. Interestingly, a similar simulation starting with a preformed transmembrane SCPN formed with **CP1** did not preserve the nanopore structure, instead the SCPN reorientated itself parallel to the membrane surface (Fig. S18). This confirms the tendency of **CP1** to form aggregates characteristic of the proposed carpet-like mechanism [19].

These results, obtained from free MD simulations, provide general information of the possible interaction mechanisms in the systems: different kind of aggregation patterns in the aqueous solution, formation of transmembrane nanotubes, self-assembly in SCPNs of different sizes in contact with the membrane surface and even the presence of free monomers in solution or interacting with the lipid bilayer. The range of simulations at different concentrations and using different membrane models as well as the reproducibility of the observed patterns supports the general trends described. However, it is not possible to discard additional interaction mechanisms that could be observed at other time scales or using different concentrations. Finally, the analysis does not show significant qualitative differences between both parameterizations, MARTINI and MA(R/S)TINI. Nevertheless, the introduc-

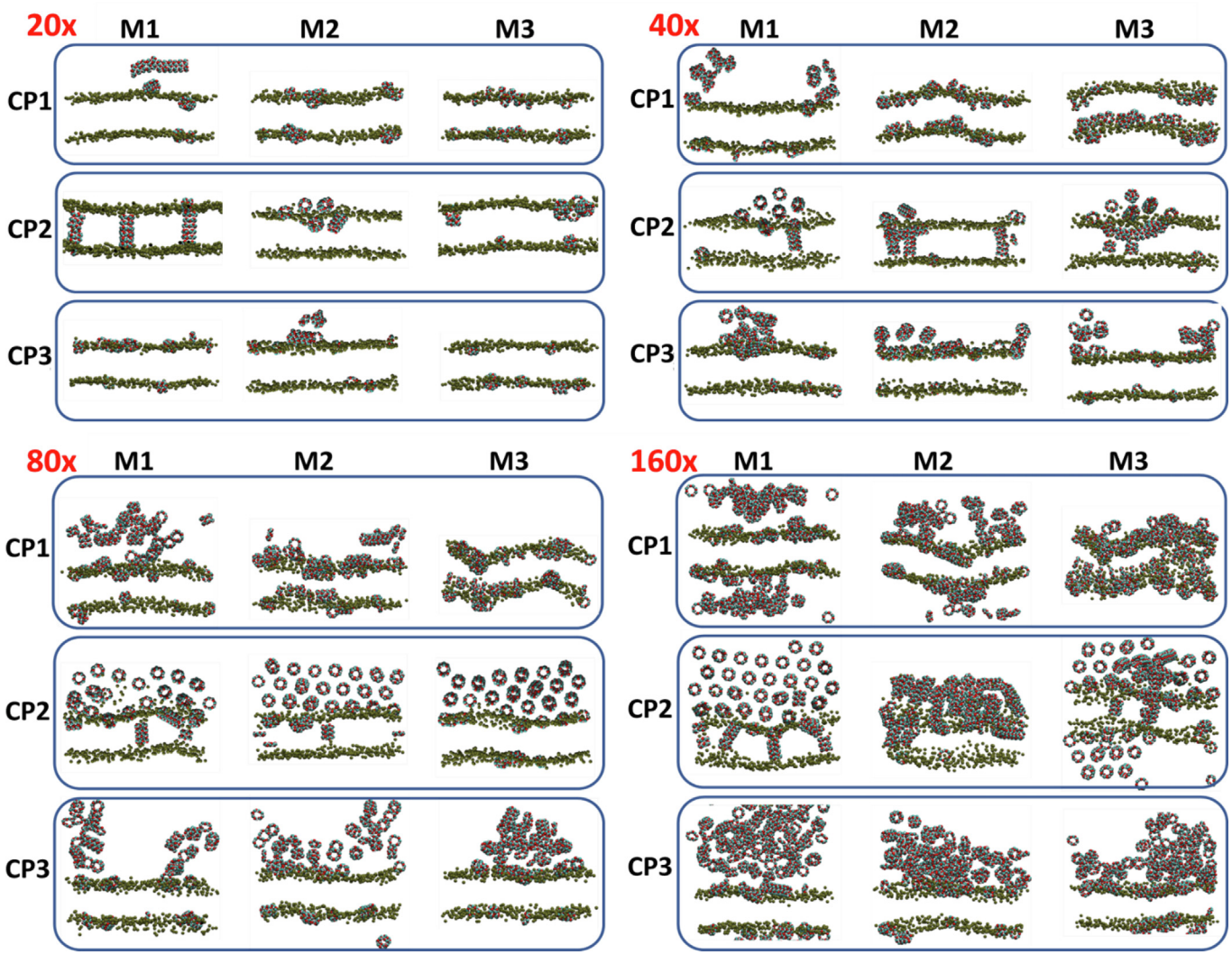

Fig. 6. Snapshots for the last frame (at 20 μs) of all the simulations performed in this work using the chirality aware MA(R/S)TINI force field. The names of the CPs and membranes are indicated in the black labels and the number of CP units for each set of simulations is indicated in the red labels. The new CPBB, CPCO and CPNH beads of the CPs are represented in cyan, red and white respectively. The beads in ochre represent the phosphate groups of the lipids. The CG beads corresponding to the lipid tails and the water have been omitted to facilitate the view. The equivalent results obtained using the original parameterization of the MARTINI model are shown in Fig. S17. (For interpretation of the references to colour in this figure legend, the reader is referred to the web version of this article.)

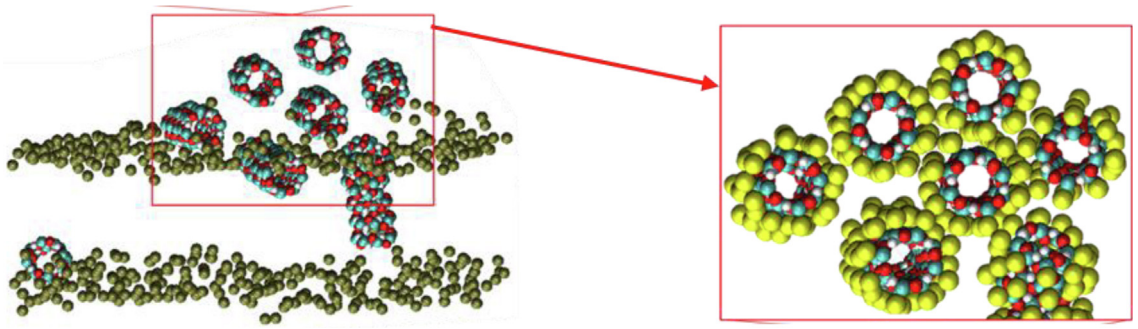

Fig. 7. Zoom in of the 2D lattice observed in the simulation of 40 **CP2** units in **M1**. The representation is equivalent to that of Fig. 8, with the beads corresponding to the leucine lateral chains in yellow spheres. (For interpretation of the references to colour in this figure legend, the reader is referred to the web version of this article.)

tion of the new beads in the MA(R/S)TINI force field allows the correct orientation of the CPs and the possibility of distinguishing between the different parallel and antiparallel arrangements along the SCPN.

3.2.3. Quantitative structural characterization of the SCPNs

The main structural parameters of the SCPNs are the distance between adjacent CPs, their relative rotational angle, and the relative orientation that determines whether they are parallel or

antiparallel to each other. The modifications introduced in the force field seriously affect these parameters. In all cases, the average CP-CP distance is reduced from an average value of 5 Å to 4.7 Å (Fig. S19-S23), which is closer to the value observed by electron diffraction and Fourier transformed infrared spectroscopy for **CP1** [9] and **CP3** [11].

The relative orientation (parallel / antiparallel) of the CPs does not seem to be seriously affected by the parameterization (Fig. S24). The results obtained for the simulations with the original parameterization of the MARTINI force field are not significantly different from those with the new MA(R/S)TINI model.

One of the most significant benefits of incorporating chirality into CP structures is the impact on the rotational angle between adjacent CPs. The new parameterization only allows four out of the eight angles observed in the original parameterization of the force field (those in which the *D*-residues are aligned - hydrogen bonded- with L-amino acids), regardless of whether the relative orientation of the CPs is parallel or antiparallel. This restriction offers improved precision and accuracy in modelling and predicting the behaviour of these chiral molecules and other forming β-sheet like structures. The probability of the different angles is different for each peptide, and it seems to be almost independent on the membrane composition present in each simulation box. This is much clearer for the MA(R/S)TINI simulations with high peptide concentrations since the number of CPs interacting is larger, thus improving the statistics and reducing the

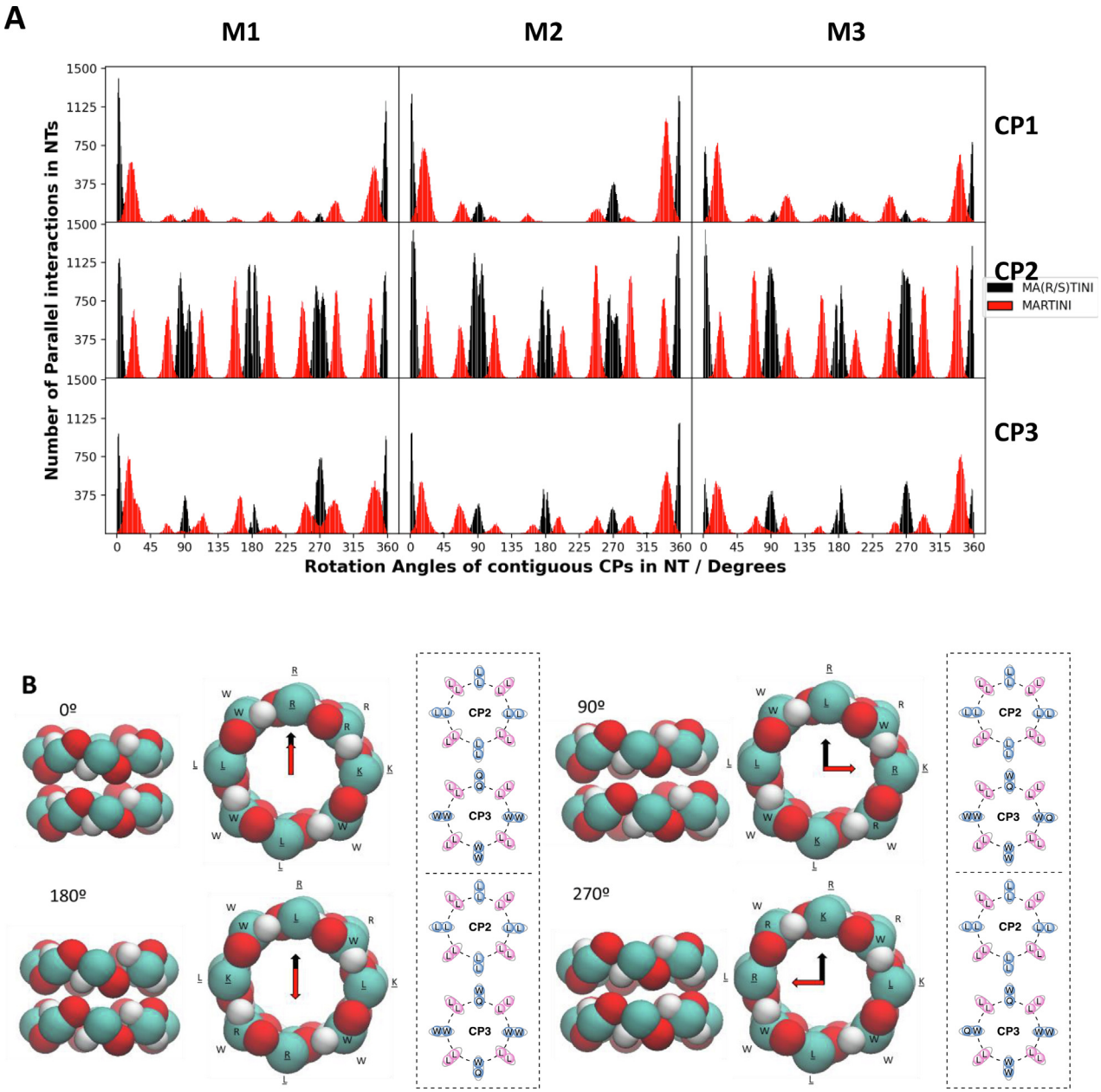

Fig. 8. A. Distribution of rotational angles for the simulations of 160 CP units in three membrane models using the original MARTINI (red) and modified MA(R/S)TINI (black) force field for **parallel** dimers. The membrane model and CP sequence are indicated in the upper and right labels. Note that the error in MARTINI is not only in the number of accessible angles but also in the centre of all distributions, which are shifted by an angle of 22.5° (π/8 rad) with respect to the correct orientation. **B**. Side and top views of parallel **CP1** dimers in MA(R/S)TINI showing selected rotational angles. Only the new CPBB, CPCO, and CPNH beads of the CPs are shown in cyan, red, and white, respectively. Analogous pictures for **CP2** and **CP3** are represented in Fig. S32-S33. The corresponding figures obtained for MARTINI are shown in Fig. S34-S36. (For interpretation of the references to colour in this figure legend, the reader is referred to the web version of this article.)

uncertainty of the results. For this reason, the following discussion will be mostly based on the simulations for the highest concentration of CP molecules (Figs. 8-9), although the general trends are also observed in the simulations with reduced number of peptide units (Figs. S25-S31). Interestingly, the differences in the rotational angles seem to depend on whether the contiguous CPs are parallel or antiparallel oriented to each other. Specifically, for both **CP1** and **CP3** the parallel orientation favours the rotamer around 0° more than the antiparallel, most likely due to a better complementarity between the interaction of the residue side chains. The presence of the rotamer around 180° (leading to the interaction between hydrophobic and hydrophilic residues) is negligible for **CP1** in the parallel orientation while the distribution over all rotamers is quite homogeneous for the antiparallel orientation of this CP (Figs. 8-9). This effect is less evident for **CP3**, although the change of distribution of rotamers between parallel and antiparallel relative orientations is also significant. As expected, **CP2** does not show any clear difference between simulations in the presence of different membrane models or relative orientations of the peptides.

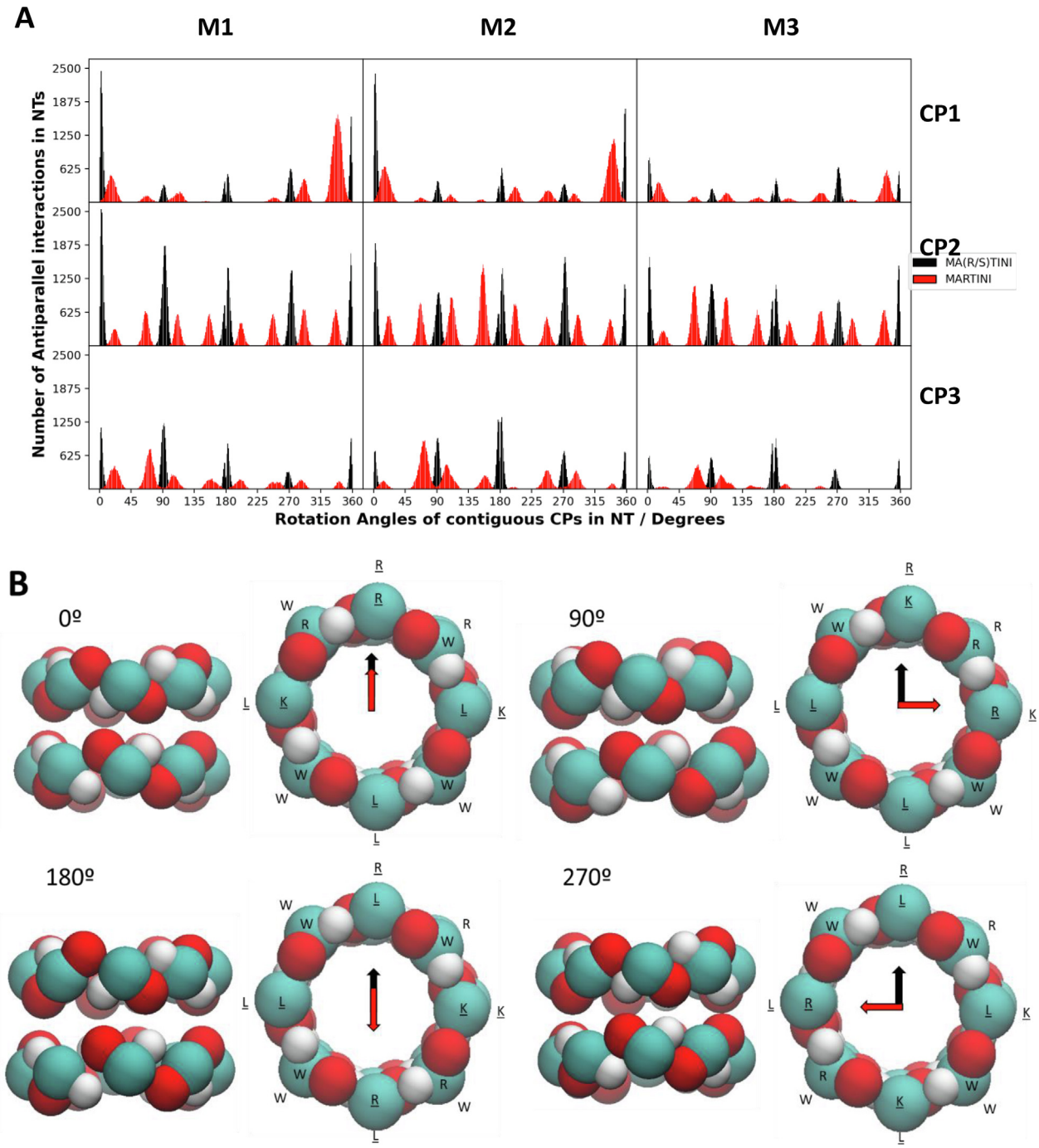

Fig. 9. A. Distribution of rotational angles for the simulations of 160 CP units in three membrane models using the original MARTINI (red) and modified MA(R/S)TINI (black) force field for **antiparallel** CP dimers. The membrane model and CP sequence are indicated in the upper and right labels. **B**. Side and top views of antiparallel **CP1** dimers in MA(R/S)TINI showing selected rotational angles. Only the new CPBB, CPCO, and CPNH beads of the CPs are shown in cyan, red, and white, respectively. Analogous pictures for **CP2** and **CP3** are represented in Fig. S32-S33. The corresponding figures obtained for MARTINI are shown in Fig. S34-S36. (For interpretation of the references to colour in this figure legend, the reader is referred to the web version of this article.)

The analysis of the rotamers for the simulations using the original MARTINI force field leads to completely different results. As anticipated, these simulations provide angles that should be structurally forbidden. The error is not only in the number of accessible angles but also in the centre of all distributions (Figs. 8-9 and S25-S31), which are shifted by 22.5° (π/8 rad) with respect to the correct orientation. This means that for a given rotamer, the optimal location of CG beads representing the backbone of the closest amino acids of contiguous CPs are not aligned along the normal to the plane of both peptides but rotated by an angle of 22.5° around the principal axis of the dimer (Fig. S32-S36). Even with these errors, there are clear differences in the rotamer profiles of the different CPs (Fig. S31). The most likely orientation for **CP1** corresponds to 338°, followed by 222° and, to a lower extent by 247° and 112°. The probability for the rest of the angles being significantly lower for all the simulations. **CP3** exhibits larger differences when using the original parameterization of the force field than when using the MA(R/S)TINI parameterization. The most probable rotamers taking place at 347° and around 22° for the parallel orientation. The impact of the relative orientation for this peptide is extremely marked, with a clear rotation towards 67° and 112° for the antiparallel orientation (Fig. S31 and S34-S36).

All the previous results indicate that the new chirality-aware parameterization, MA(R/S)TINI, improves the structural results obtained for the self-assembly of individual CPs into SCPNs. The new parameterization resulted in improved agreement between the simulated and experimental CP-CP distances, more reasonable rotational angles, and more consistent angle distributions across different simulations at various concentrations and in the presence of different membrane models. This helps to ensure that the assemblies formed during the simulations are feasible.

4. Conclusions

The MARTINI force field is a powerful model for simulating biological systems at a coarse-grained level. Using this model, it is possible to study the self-assembly of a variety of molecules into reliable supramolecular patterns. However, the original form of the MARTINI force field is not able to accurately describe the interactions that lead to the formation of protein or peptide secondary structures. Even the last version of the force field [30], which introduces new particles and features with respect to previous versions, represents the backbone residues using a single bead, which does not allow to consider the directionality of the H-bonds required to correctly establish the chirality of these groups. This limitation becomes particularly important when studying *D*, *L*-α-CPs, which have a critical *D*- and *L*-chirality sequential fluctuation that affects their disposition into SCPNs. The self-assembly of *D*,*L*-α-CPs using the unmodified versions of the MARTINI CG model results in a misrepresentation of reality, as it does not properly account for relative amino acid chirality and for the parallel and antiparallel beta-sheets that can form along the SCPN. Additionally, the MARTINI model overestimates the interaction between the beads that represent the backbone atoms of contiguous parallel or antiparallel CPs. This allows stacking patterns that should not be feasible because of the unmatching between donor and acceptor groups of both peptide strands as a consequence of the alternating chirality.

D,*L*-CPs have the potential to be used in many biological and biotechnological applications, mainly due to capability of tunning the external properties to favour interactions with other entities, such as lipid bilayers of different compositions and mechanisms of interaction with the membrane depending on their sequence. To better understand the properties of different CPs and their interactions with membrane models, we have introduced a new parameterization of the MARTINI 2.2 force field, called MA(R/S)TINI. This chirality aware new model solves the most evident issues of the original parameterization. The optimized model is tested using three CPs evaluating their contact with three membrane models. The three CPs have 8 amino acids but different expected behaviour in the presence of lipid bilayers. **CP1** is amphipathic, with a total positive charge of +3e and with demonstrated antibacterial activity, **CP2** is a model structure consisting of 8 leucine residues, and **CP3** is mostly hydrophobic. They were simulated in presence of a simplified mammalian membrane (**M1**), and two bacterial membrane models (**M2** and **M3**) with different negative charge density (**M2** < **M3**). Both MARTINI and MA(R/S)TINI parameterizations produced similar aggregation patterns as well as equivalent interaction mechanisms with the different lipid bilayers. **CP1** clearly perturb the structure of the membranes at high concentration, while **CP2** forms 2D lattices and transmembrane nanotubes. **CP3** forms aggregates in the water solution, probably because it is highly hydrophobic, and it is not able to traverse the energy barrier represented by the lipid heads. **CP1** and **CP3** typically form small aggregates and, even at high concentration, many of these peptides remain as isolated monomers. In contrast, **CP2** forms larger aggregates with just a marginal presence of monomers, which could be related to its low solubility. The kinetic behaviour of the three peptides is also interesting, the formation of **CP2** aggregates being much faster than that of **CP1** and **CP3**. The time scale required to form stable aggregates is typically of just 1–2 μs for **CP2**, 2–4 μs for **CP3** and 4–7 μs for **CP1**. When looking into detail at the interactions between consecutive CPs in the aggregates the results were very clear in favour of the new parameterization, which was able to reproduce the distance between CPs interacting in parallel and antiparallel orientation, as well as the correct rotational angles and energy profiles. Additionally, in contrast with the original force field parameterization, the simulations with MA(R/S)TINI were able to distinguish the different relative orientation of the peptides (parallel or antiparallel).

When analysing the interactions between consecutive CPs in the aggregates, the results were overwhelmingly in favour of the new parameterization. The MA(R/S)TINI model was able to accurately reproduce the distance between CPs interacting in parallel and antiparallel orientations, as well as the correct rotational angles and energy profiles. Furthermore, unlike the original force field parameterization, MA(R/S)TINI was able to distinguish the different relative orientations of the peptides (parallel or antiparallel), avoiding the forbidden rotational angles that were present in the original MARTINI model. These results are supported by the known and expected behaviour of the studied CPs and membrane models. Further validations and improvements in the MA(R/S)TINI model can still be performed. This would require more detailed quantitative experimental information such as energy of interaction for different sequences in different relative orientations. Additionally, in this study, the MARTINI 2.2 force field was selected as the reference to develop the personalized adaptation for cyclic peptides, despite the availability of the more versatile and accurate MARTINI 3.0. This decision was made as the initiation of the project preceded the publication of last version of the force field and the trial and error process, along with the production of results for all systems, was a long process. Anyway, the essential aspect of both MARTINI 2.2 and 3.0 parameterizations are equivalent in regards to the modifications introduced in this manuscript. Both parameterizations represent the amino acid backbone using a single bead, making the adaptations introduced in this work crucial for accurate parameterization of cyclic peptides.

The observed strong perturbation of **M2** and **M3**, and not of **M1**, by **CP1** should be clearly connected to its known antibacterial activity [15,38]. Other CP sequences have been observed to form 2D lattices and transmembrane nanotubes, similarly to **CP2** [59].

For **CP3** we expected to see also the formation of transmembrane SCPNs due to its hydrophobic nature but the presence of the lipid heads could prevent the penetration of this peptide in the hydrophobic region of the membrane, thus favouring its self-aggregation in the aqueous bulk [11]. The new parameterization of the MARTINI force field, MA(R/S)TINI, opens the door to computationally characterizing the dynamic behaviour of CPs in contact with membrane models in a more efficient way, thus facilitating the design of new functional sequences. In addition, a web application (https://cyclopep.com) is being developed to automatically generate CP structures and the corresponding MA(R/S)TINI parameters for any sequence of natural amino acids, among other functionalities.

CRediT authorship contribution statement

Rebeca Garcia-Fandino: Conceptualization, Funding acquisition, Investigation, Methodology, Project administration, Supervision, Writing. **Ángel Piñeiro:** Conceptualization, Funding acquisition, Investigation, Methodology, Project administration, Supervision, Writing.

Declaration of Competing Interest

The authors declare that they have no known competing financial interests or personal relationships that could have appeared to influence the work reported in this paper.

Data availability

Data will be made available on request.

Acknowledgements

This work was supported by the Spanish Agencia Estatal de Investigación (AEI) (RTI2018-098795-A-I00, PID2019-111327GB-I00, PID2019-111126RB-100 and PDC2022-133402-I00), by Xunta de Galicia (ED431F 2020/05, ED431B 2022/36, ED431C 2017/25 and Centro singular de investigación de Galicia accreditation 2019-2022, ED431G 2019/03) and the European Union (European Regional Development Fund - ERDF). R.G.-F. thanks Ministerio de Ciencia, Innovación y Universidades for a "Ramón y Cajal" contract (RYC-2016-20335). All calculations were carried out at the Centro de Supercomputación de Galicia (CESGA).

Appendix A. Supplementary data

Figures S1-S35. The topologies, coordinates, and input software files (with top, itp, gro and mdp extensions for GROMACS) required to perform the simulations are directly available from Zenodo. Supplementary data to this article can be found online at https://doi.org/10.1016/j.jcis.2023.03.101.

References

[1] D. Pochan, O. Scherman, Introduction: Molecular Self-Assembly, Chem. Rev. (2021) 13699–13700, https://doi.org/10.1021/acs.chemrev.1c00884.
[2] A.C. Mendes, E.T. Baran, R.L. Reis, H.S. Azevedo, Self-Assembly in Nature: Using the Principles of Nature to Create Complex Nanobiomaterials, Wiley Interdiscip. Rev. Nanomedicine Nanobiotechnology 5 (6) (2013) 582–612, https://doi.org/10.1002/wnan.1238.
[3] S. La Manna, C. Di Natale, V. Onesto, D. Marasco, Self-Assembling Peptides: From Design to Biomedical Applications, Int. J. Mol. Sci. (2021) 12662, https://doi.org/10.3390/ijms222312662.
[4] A. Levin, T.A. Hakala, L. Schnaider, G.J.L. Bernardes, E. Gazit, T.P.J. Knowles, Biomimetic Peptide Self-Assembly for Functional Materials, Nat. Rev. Chem. (2020) 615–634, https://doi.org/10.1038/s41570-020-0215-y.
[5] B. Claro, M. Bastos, R. Garcia-Fandino, Design and Applications of Cyclic Peptides, in: Peptide Applications in Biomedicine, Biotechnology and Bioengineering, Woodhead Publishing, 2018, pp. 87–129, https://doi.org/10.1016/B978-0-08-100736-5.00004-1.
[6] A. Méndez-Ardoy, I. Insua, J.R. Granja, J. Montenegro, Cyclization and Self-Assembly of Cyclic Peptides, in: Methods in Molecular Biology, vol. 2371, Humana, New York, NY, 2022, pp. 449-466. Doi: 10.1007/978-1-0716-1689-5_24.
[7] Q. Song, Z. Cheng, M. Kariuki, S.C.L. Hall, S.K. Hill, J.Y. Rho, S. Perrier, Molecular Self-Assembly and Supramolecular Chemistry of Cyclic Peptides, Chem. Rev. (2021) 13936–13995, https://doi.org/10.1021/acs.chemrev.0c01291.
[8] P. De Santis, S. Morosetti, R. Rizzo, Conformational Analysis of Regular Enantiomeric Sequences, Macromolecules 7 (1) (1974) 52–58, https://doi.org/10.1021/ma60037a011.
[9] M.R. Ghadiri, J.R. Granja, R.A. Milligan, D.E. McRee, N. Khazanovich, Self-Assembling Organic Nanotubes Based on a Cyclic Peptide Architecture, Nature 366 (6453) (1993) 324–327, https://doi.org/10.1038/366324a0.
[10] N. Rodriguez-Vazquez, H. Ozores, A. Guerra, E. Gonzalez-Freire, A. Fuertes, M. Panciera, J. Priegue, J. Outeiral, J. Montenegro, R. Garcia-Fandino, M. Amorin, J. Granja, Membrane-Targeted Self-Assembling Cyclic Peptide Nanotubes, Curr. Top. Med. Chem. 14 (23) (2015) 2647–2661, https://doi.org/10.2174/1568026614666141215143431.
[11] M.R. Ghadiri, J.R. Granja, L.K. Buehler, Artificial Transmembrane Ion Channels from Self-Assembling Peptide Nanotubes, Nature 369 (6478) (1994) 301–304, https://doi.org/10.1038/369301a0.
[12] J. Montenegro, M.R. Ghadiri, J.R. Granja, Ion Channel Models Based on Self-Assembling Cyclic Peptide Nanotubes, Acc. Chem. Res. 46 (12) (2013) 2955–2965, https://doi.org/10.1021/ar400061d.
[13] B. Claro, E. González-Freire, J.R. Granja, R. Garcia-Fandiño, J. Gallová, D. Uhríková, A. Fedorov, A. Coutinho, M. Bastos, Partition of Antimicrobial D-L-α-Cyclic Peptides into Bacterial Model Membranes, Biochim. Biophys. Acta - Biomembr. 1864 (1) (2022), https://doi.org/10.1016/J.BBAMEM.2021.183729 183729.
[14] B. Claro, A. Peón, E. González-Freire, E. Goormaghtigh, M. Amorín, J.R. Granja, R. Garcia-Fandiño, M. Bastos, Macromolecular Assembly and Membrane Activity of Antimicrobial D, L-α-Cyclic Peptides, Colloid Surf. B 208 (2021), https://doi.org/10.1016/J.COLSURFB.2021.112086 112086.
[15] B. Claro, E. González-Freire, M. Calvelo, L.J. Bessa, E. Goormaghtigh, M. Amorín, J.R. Granja, R. Garcia-Fandiño, M. Bastos, Membrane Targeting Antimicrobial Cyclic Peptide Nanotubes - an Experimental and Computational Study, Colloid Surf. B 196 (2020), https://doi.org/10.1016/j.colsurfb.2020.111349 111349.
[16] P.W.J.M. Frederix, I. Patmanidis, S.J. Marrink, Molecular Simulations of Self-Assembling Bio-Inspired Supramolecular Systems and Their Connection to Experiments, Chem. Soc. Rev. (2018) 3470–3489, https://doi.org/10.1039/c8cs00040a.
[17] M. Orsi, Molecular Simulation of Self-Assembly. In Self-Assembling Biomaterials: Molecular Design, Characterization and Application in Biology and Medicine, Woodhead Publishing, 2018, pp. 305–318.
[18] A. Blanco-González, M. Calvelo, P.F. Garrido, M. Amorín, J.R. Granja, Á. Piñeiro, R. Garcia-Fandino, Transmembrane Self-Assembled Cyclic Peptide Nanotubes Based on Α-Residues and Cyclic Δ-Amino Acids: A Computational Study, Front. Chem. 9 (2021) 530, https://doi.org/10.3389/fchem.2021.704160.
[19] R. Garcia-Fandiño, Á. Piñeiro, J.L. Trick, M.S.P. Sansom, Lipid Bilayer Membrane Perturbation by Embedded Nanopores: A Simulation Study, ACS Nano 10 (3) (2016) 3693–3701, https://doi.org/10.1021/acsnano.6b00202.
[20] R. Garcia-Fandiño, M. Calvelo, J.R. Granja, Pore- and Channel-Forming Peptides and Their Mimetics, Comprehensive Supramolecular Chemistry II, Vol. 4, Elsevier Inc., 2017, pp. 539–573, https://doi.org/10.1016/B978-0-12-409547-2.12546-6.
[21] D. Conde, P.F. Garrido, M. Calvelo, Á. Piñeiro, R. Garcia-Fandiño, Molecular Dynamics Simulations of Transmembrane Cyclic Peptide Nanotubes Using Classical Force Fields, Hydrogen Mass Repartitioning and Hydrogen Isotope Exchange Methods: A Critical Comparison, Int. J. Mol. Sci. 23 (6) (2022) 3158, https://doi.org/10.3390/ijms23063158.
[22] M. Calvelo, J.R. Granja, R. Garcia-Fandino, Competitive Double-Switched Self-Assembled Cyclic Peptide Nanotubes: A Dual Internal and External Control, Phys. Chem. Chem. Phys. 21 (37) (2019) 20750–20756, https://doi.org/10.1039/c9cp02327e.
[23] M. Calvelo, C.I. Lynch, J.R. Granja, M.S.P. Sansom, R. Garcia-Fandiño, Effect of Water Models on Transmembrane Self-Assembled Cyclic Peptide Nanotubes, ACS Nano 15 (4) (2021) 7053–7064, https://doi.org/10.1021/acsnano.1c00155.
[24] R. García-Fandiño, J.R. Granja, Effect of Organochloride Guest Molecules on the Stability of Homo/Hetero Self-Assembled α, γ-Cyclic Peptide Structures: A Computational Study toward the Control of Nanotube Length, J. Phys. Chem. C 117 (19) (2013) 10143–10162, https://doi.org/10.1021/jp400796n.
[25] R. García-Fandiño, M.S.P. Sansom, Designing Biomimetic Pores Based on Carbon Nanotubes, Proc. Natl. Acad. Sci. U. S. A. 109 (18) (2012) 6939–6944, https://doi.org/10.1073/pnas.1119326109.
[26] P. Brocos, P. Mendoza-Espinosa, R. Castillo, J. Mas-Oliva, Á. Piñeiro, Multiscale Molecular Dynamics Simulations of Micelles: Coarse-Grain for Self-Assembly and Atomic Resolution for Finer Details, Soft Matter 8 (34) (2012) 9005–9014, https://doi.org/10.1039/c2sm25877c.
[27] E. Panizon, D. Bochicchio, L. Monticelli, G. Rossi, MARTINI Coarse-Grained Models of Polyethylene and Polypropylene, J. Phys. Chem. B 119 (25) (2015) 8209–8216, https://doi.org/10.1021/acs.jpcb.5b03611.

[28] C.A. López, A.J. Rzepiela, A.H. de Vries, L. Dijkhuizen, P.H. Hünenberger, S.J. Marrink, Martini Coarse-Grained Force Field: Extension to Carbohydrates, J. Chem. Theory Comput. 5 (12) (2009) 3195–3210, https://doi.org/10.1021/ct900313w.
[29] L. Monticelli, S.K. Kandasamy, X. Periole, R.G. Larson, D.P. Tieleman, S.J. Marrink, The MARTINI Coarse-Grained Force Field: Extension to Proteins, J. Chem. Theory Comput. 4 (5) (2008) 819–834, https://doi.org/10.1021/ct700324x.
[30] P.C.T. Souza, R. Alessandri, J. Barnoud, S. Thallmair, I. Faustino, F. Grünewald, I. Patmanidis, H. Abdizadeh, B.M.H. Bruininks, T.A. Wassenaar, P.C. Kroon, J. Melcr, V. Nieto, V. Corradi, H.M. Khan, J. Domański, M. Javanainen, H. Martinez-Seara, N. Reuter, R.B. Best, I. Vattulainen, L. Monticelli, X. Periole, D.P. Tieleman, A.H. de Vries, S.J. Marrink, Martini 3: A General Purpose Force Field for Coarse-Grained Molecular Dynamics, Nat. Methods 18 (4) (2021) 382–388, https://doi.org/10.1038/s41592-021-01098-3.
[31] D.H. De Jong, G. Singh, W.F.D. Bennett, C. Arnarez, T.A. Wassenaar, L.V. Schäfer, X. Periole, D.P. Tieleman, S.J. Marrink, Improved Parameters for the Martini Coarse-Grained Protein Force Field, J. Chem. Theory Comput. 9 (1) (2013) 687–697, https://doi.org/10.1021/ct300646g.
[32] S.J. Marrink, L. Monticelli, M.N. Melo, R. Alessandri, D.P. Tieleman, P.C.T. Souza, Two Decades of Martini: Better Beads, Broader Scope, Wiley Interdiscip. Rev.: Comput. Mol. Sci. John Wiley & Sons, Ltd (2022) e1620.
[33] S.J. Marrink, H.J. Risselada, S. Yefimov, D.P. Tieleman, A.H. De Vries, The MARTINI Force Field: Coarse Grained Model for Biomolecular Simulations, J. Phys. Chem. B 111 (27) (2007) 7812–7824, https://doi.org/10.1021/jp071097f.
[34] C. Wang, L. Guan, D. Danovich, S. Shaik, Y. Mo, The Origins of the Directionality of Noncovalent Intermolecular Interactions, J. Comput. Chem. 37 (1) (2016) 34–45, https://doi.org/10.1002/jcc.23946.
[35] P. Tiangtrong, N. Thamwattana, D. Baowan, Modelling Water Molecules inside Cyclic Peptide Nanotubes, Appl. Nanosci. 6 (3) (2016) 345–357, https://doi.org/10.1007/s13204-015-0436-4.
[36] M. Tarek, B. Maigret, C. Chipot, Molecular Dynamics Investigation of an Oriented Cyclic Peptide Nanotube in DMPC Bilayers, Biophys. J. 85 (4) (2003) 2287–2298, https://doi.org/10.1016/S0006-3495(03)74653-0.
[37] A. Khalfa, M. Tarek, On the Antibacterial Action of Cyclic Peptides: Insights from Coarse-Grained MD Simulations, J. Phys. Chem. B 114 (8) (2010) 2676–2684, https://doi.org/10.1021/jp9064196.
[38] S. Fernandez-Lopez, H.S. Kim, E.C. Choi, M. Delgado, J.R. Granja, A. Khasanov, K. Kraehenbuehl, G. Long, D.A. Weinberger, K.M. Wilcoxen, M.R. Ghadiri, Antibacterial Agents Based on the Cyclic D,L-α-Peptide Architecture, Nature 412 (6845) (2001) 452–455, https://doi.org/10.1038/35086601.
[39] G. Van Meer, D.R. Voelker, G.W. Feigenson, Membrane Lipids: Where They Are and How They Behave, Nat. Rev. Mol. Cell Bio. (2008) 112–124, https://doi.org/10.1038/nrm2330.
[40] G. Shahane, W. Ding, M. Palaiokostas, M. Orsi, Physical Properties of Model Biological Lipid Bilayers: Insights from All-Atom Molecular Dynamics Simulations, J. Mol. Model. 25 (3) (2019) 1–13, https://doi.org/10.1007/s00894-019-3964-0.
[41] K. Murzyn, T. Róg, M. Pasenkiewicz-Gierula, Phosphatidylethanolamine-Phosphatidylglycerol Bilayer as a Model of the Inner Bacterial Membrane, Biophys. J. 88 (2) (2005) 1091–1103, https://doi.org/10.1529/biophysj.104.048835.
[42] M.Z. Tien, D.K. Sydykova, A.G. Meyer, C.O. Wilke, Peptidebuilder: A Simple Python Library to Generate Model Peptides, PeerJ 2013 (1) (2013) e80.
[43] P. Gkeka, L. Sarkisov, Interactions of Phospholipid Bilayers with Several Classes of Amphiphilic α-Helical Peptides: Insights from Coarse-Grained Molecular Dynamics Simulations, J. Phys. Chem. B 114 (2010) 826–839, https://doi.org/10.1021/jp908320b.
[44] M.J. Abraham, T. Murtola, R. Schulz, S. Páll, J.C. Smith, B. Hess, E. Lindah, Gromacs: High Performance Molecular Simulations through Multi-Level Parallelism from Laptops to Supercomputers, SoftwareX 1–2 (2015) 19–25, https://doi.org/10.1016/j.softx.2015.06.001.
[45] Y. Qi, H.I. Ingólfsson, X. Cheng, J. Lee, S.J. Marrink, W. Im, CHARMM-GUI Martini Maker for Coarse-Grained Simulations with the Martini Force Field, J. Chem. Theory Comput. 11 (9) (2015) 4486–4494, https://doi.org/10.1021/acs.jctc.5b00513.
[46] H.J.C. Berendsen, J.P.M. van Postma, W.F. van Gunsteren, A. DiNola, J.R. Haak, Molecular Dynamics with Coupling to an External Bath, J. Chem. Phys. 81 (8) (1984) 3684–3690.
[47] M. Parrinello, A. Rahman, Polymorphic Transitions in Single Crystals: A New Molecular Dynamics Method, J. Appl. Phys. 52 (12) (1981) 7182–7190, https://doi.org/10.1063/1.328693.
[48] G. Bussi, D. Donadio, M. Parrinello, Canonical Sampling through Velocity Rescaling, J. Chem. Phys. 126 (1) (2007), https://doi.org/10.1063/1.2408420 014101.
[49] B. Hess, H. Bekker, H.J.C. Berendsen, J.G.E.M. Fraaije, LINCS: A Linear Constraint Solver for Molecular Simulations, J. Comput. Chem. 18 (18) (1997) 1463–1472, https://doi.org/10.1002/(SICI)1096-987X(199709)18:12<1463::AID-JCC4>3.0.CO;2-H.
[50] U. Essmann, L. Perera, M.L. Berkowitz, T. Darden, H. Lee, L.G. Pedersen, A Smooth Particle Mesh Ewald Method, J. Chem. Phys. 103 (19) (1995) 8577–8593, https://doi.org/10.1063/1.470117.
[51] S.O. Yesylevskyy, L.V. Schäfer, D. Sengupta, S.J. Marrink, Polarizable Water Model for the Coarse-Grained MARTINI Force Field, PLoS Comput. Biol. 6 (6) (2010) 1–17, https://doi.org/10.1371/journal.pcbi.1000810.
[52] A. Lindahl, S.V. de Hess, GROMACS 2021 Manual. Zenodo. GROMACS 2021 Manual. Zenodo 2021.
[53] M. Bonomi, G. Bussi, C. Camilloni, G.A. Tribello, P. Banáš, A. Barducci, M. Bernetti, P.G. Bolhuis, S. Bottaro, D. Branduardi, R. Capelli, P. Carloni, M. Ceriotti, A. Cesari, H. Chen, W. Chen, F. Colizzi, S. De, M. De La Pierre, D. Donadio, V. Drobot, B. Ensing, A.L. Ferguson, M. Filizola, J.S. Fraser, H. Fu, P. Gasparotto, F.L. Gervasio, F. Giberti, A. Gil-Ley, T. Giorgino, G.T. Heller, G.M. Hocky, M. Iannuzzi, M. Invernizzi, K.E. Jelfs, A. Jussupow, E. Kirilin, A. Laio, V. Limongelli, K. Lindorff-Larsen, T. Löhr, F. Marinelli, L. Martin-Samos, M. Masetti, R. Meyer, A. Michaelides, C. Molteni, T. Morishita, M. Nava, C. Paissoni, E. Papaleo, M. Parrinello, J. Pfaendtner, P. Piaggi, G.M. Piccini, A. Pietropaolo, F. Pietrucci, S. Pipolo, D. Provasi, D. Quigley, P. Raiteri, S. Raniolo, J. Rydzewski, M. Salvalaglio, G.C. Sosso, V. Spiwok, J. Šponer, D.W.H. Swenson, P. Tiwary, O. Valsson, M. Vendruscolo, G.A. Voth, A. White, Promoting Transparency and Reproducibility in Enhanced Molecular Simulations, Nat. Methods (2019) 670–673, https://doi.org/10.1038/s41592-019-0506-8.
[54] W. Humphrey, A. Dalke, K. Schulten, VMD: Visual Molecular Dynamics, J. Mol. Graph. 14 (1) (1996) 33–38, https://doi.org/10.1016/0263-7855(96)00018-5.
[55] N. Michaud-Agrawal, E.J. Denning, T.B. Woolf, O. Beckstein, MDAnalysis: A Toolkit for the Analysis of Molecular Dynamics Simulations, J. Comput. Chem. 32 (10) (2011) 2319–2327, https://doi.org/10.1002/jcc.21787.
[56] C.R. Harris, K.J. Millman, S.J. van der Walt, R. Gommers, P. Virtanen, D. Cournapeau, E. Wieser, J. Taylor, S. Berg, N.J. Smith, R. Kern, M. Picus, S. Hoyer, M.H. van Kerkwijk, M. Brett, A. Haldane, J.F. del Río, M. Wiebe, P. Peterson, P. Gérard-Marchant, K. Sheppard, T. Reddy, W. Weckesser, H. Abbasi, C. Gohlke, T.E. Oliphant, Array Programming with NumPy, Nature (2020) 357–362, https://doi.org/10.1038/s41586-020-2649-2.
[57] J.D. Hunter, Matplotlib: A 2D Graphics Environment, Comput. Sci. Eng. 9 (3) (2007) 90–95, https://doi.org/10.1109/MCSE.2007.55.
[58] This type of peptides is very poorly soluble in water and tends to precipitate as soon as CP solutions in DMSO are added to aqueous solutions containing liposomes, so their behavior as transmembrane channel formers is unknown (*unpublished results*).
[59] I. Insua, J. Montenegro, 1D to 2D Self Assembly of Cyclic Peptides, J. Am. Chem. Soc. 142 (1) (2020) 300–307, https://doi.org/10.1021/jacs.9b10582.